Proceedings of the
Annual Stability Conference
Structural Stability Research Council
St. Louis, Missouri, April 2-5, 2019

Post-buckling behavior of thin-walled regular polygonal tubular columns undergoing local-distortional interaction

André D. Martins[1], Rodrigo Gonçalves[2], Dinar Camotim[3]

Abstract

This work presents and discusses numerical results of an ongoing investigation concerning the elastic post-buckling behavior and imperfection sensitivity of regular convex polygonal cross-section (RCPS) tubular columns affected by local-distortional (L-D) interaction. This investigation is conducted by means of geometrically non-linear Generalized Beam Theory (GBT) analyses, extending the knowledge on the "pure" local and distortional post-buckling behaviors of RCPS tubes recently reported by the authors (Martins *et al*. 2018a). Due to their inherent modal nature, the GBT analyses make it possible to acquire in-depth knowledge on the structural behavior of RCPS tubes and also to include, in a straightforward fashion, arbitrary member initial geometrical imperfections. Columns with distortional-to-local critical buckling load ratios (i) close to 1 ("true L-D interaction" – the most trivial L-D interaction type) and (ii) significantly above 1 ("secondary-distortional bifurcation L-D interaction" – the most relevant L-D interaction type) are investigated. Local/distortional critical-mode initial geometrical imperfections and (linear) combinations of both are considered in the former columns, while only local initial imperfections are dealt with in the latter ones – several amplitudes are dealt with to assess the imperfection sensitivity. For comparison and validation purposes, ABAQUS shell finite element analysis results are also reported.

1. Introduction

Thin-walled tubes with regular convex polygonal cross-sections (RCPS) are widely used in the construction industry, namely in communication towers and posts supporting lighting equipment or overhead power lines. As open-section thin-walled members, polygonal tubes may also be affected by several instability phenomena, involving individual (local, distortional or global) and/or coupled (local-global, local-distortional, distortional-global or local-distortional-global) buckling behaviors. Indeed, it is fair to state that most of the knowledge concerning this peculiar cross-section type is associated with the local buckling and post-buckling behaviors (Timoshenko & Gere 1961, Wittrick & Curzon 1968) and is already adequately reflected in the current design specifications worldwide. However, the same is not true for distortional and coupling phenomena of RCPS members – therefore, research on these structural behaviors is still needed.

[1] Postdoctoral Researcher, CERIS, DECivil, Instituto Superior Técnico, Universidade de Lisboa, <andrerdmartins@ist.utl.pt>

[2] Associate Professor, CERIS, DEC, Faculdade de Ciências e Tecnologia, Universidade Nova de Lisboa, <rodrigo.goncalves@fct.unl.pt>

[3] Professor, CERIS, DECivil, Instituto Superior Técnico, Universidade de Lisboa, <dcamotim@civil.ist.utl.pt>

In order to contribute towards bridging this gap, the authors carried out, in the last few years, an in-depth investigation aimed at characterizing the structural behavior of RCPS tubular members, taking advantage of the unique modal decomposition features provided by Generalized Beam Theory (GBT) – *e.g.*, Schardt (1989), Camotim *et al*. (2010a,b), Gonçalves *et al*. (2010), Gonçalves & Camotim (2012). Indeed, Gonçalves & Camotim (2013a) proposed a novel cross-section analysis procedure (to determine the deformation modes), based on a "GBT specialization" that accounts for the cross-section rotational symmetry exhibited by the RCPS (of order equal to the number of walls), which makes it possible to orthogonalize almost all the deformation mode sets. It was also shown that a single deformation mode pair often provides the solution for a given structural problem – this implies that this "GBT specialization" leads to significant computational savings and provides added insight on the RCPS member response. The novel procedure was validated and employed to perform first-order (Gonçalves & Camotim 2013a), vibration (Gonçalves & Camotim 2014) and buckling analyses of prismatic thin-walled tubes – in the last case, tubes under compression (Gonçalves & Camotim 2013b) and bending and torsion (Gonçalves & Camotim 2013c). A summary of the research work carried out on the GBT analysis of RCPS tubes can be found in Gonçalves & Camotim (2016). These investigations unveiled striking and surprisingly peculiar behavioral features, namely that RCPS members (i) may be susceptible to cross-section distortion (in-plane and out-of-plane deformation), which may govern the strength of "intermediate-length" columns, (ii) exhibit duplicate local and distortional buckling (as well as vibration) modes for a wide range of geometries with practical interest, due to the cross-section rotational symmetry. Recently, Martins *et al*. (2018a) investigated the local and (mostly) distortional post-buckling behaviors of RCPS columns. They found that the local post-buckling response is highly stable and unaffected by the existence of duplicate buckling modes, while the distortional post-buckling behavior is slightly unstable and exhibits secondary equilibrium paths along the primary descending branch. While one of those paths involves a localized phenomenon/kink and is only detectable by resorting to branch switching techniques, the other path is associated with column deformed configurations that become progressively more "ovalized".

Naturally, the next step of our research effort consisted of studying RCPS columns experiencing local-distortional (L-D) interaction and the results obtained so far are presented and discussed in this paper. At this stage, it is worth mentioning that, to the authors' best knowledge, there is no available research work on the influence of local-distortional interaction in the behavior and strength of RCPS columns. Indeed, most of the available investigations on this type of interaction concern almost exclusively lipped open-section thin-walled columns, which exhibit stable local and distortional post-buckling behaviors, (highly and moderately, respectively) – see, for instance the recently GBT investigations concerning (i) simply supported and fixed-ended lipped channel columns (Martins *et al*. 2018b) and (ii) simply supported uniformly bent lipped channel beams (Martins *et al*. 2018c) undergoing local-distortional interaction.

Therefore, this paper presents and discusses numerical results about the elastic post-buckling behavior and imperfection sensitivity of RCPS columns affected by L-D interaction, which are obtained by means of geometrically non-linear GBT analyses (Martins *et al.* 2018d). After addressing the buckling behavior of the RCPS column selection, in Section 2, the corresponding post-buckling behavior is presented and discussed in Section 3 (main section). In particular, columns with distortional-to-local critical buckling load ratios (i) close to 1 ("true L-D interaction") and (ii) significantly above 1 ("secondary-distortional bifurcation L-D interaction") are analyzed. Local and distortional critical-mode initial geometrical imperfections, as well as combinations of both, are incorporated into the former columns, while the latter contain only local initial imperfections – several amplitudes are considered, in order to assess the imperfection sensitivity. Finally, the paper closes with the list of the most relevant conclusions drawn from this investigation.

It is still worth mentioning that this investigation is carried out in the context of the Research Fund for Coal and Steel (RFCS) project RFCS-2015-709892, "Overall-Slenderness Based Direct Design for Strength and Stability of Innovative Hollow Sections" (HOLLOSSTAB), which is funded by the European Commission.

2. Buckling Behavior

This section describes and characterizes the buckling (linear stability) behavior of the columns prone to L-D interaction, which are analyzed in Section 3. Two RCPS simply supported (end cross-sections locally/globally pinned and free to warp) columns geometries (cross-section dimensions and lengths) are selected, associated with distinct structural mechanics, in the sense that they are characterized by distortional-to-local critical buckling load ratios (i) close to 1, corresponding to "true L-D interaction", and (ii) equal to 2.5, corresponding to "secondary-distortional bifurcation L-D interaction" (L-D is expected to occur only at advanced loading stages) – the latter case ($P_{crL}<P_{crD}$) is clearly more relevant for design purposes, since it covers a much larger number of column geometries[4]. As done in previous studies, this column geometry selection was made by means of a "trial-and-error" procedure involving GBT buckling analysis sequences performed with the GBTUL code (Bebiano *et al*. 2018), which is based on the cross-section analysis developed by Gonçalves *et al*. (2014) and Bebiano *et al*. (2015). Table 1 shows the output of this effort: (i) two column cross-section dimensions (b, R, t – wall width, circumradius and wall thickness) and lengths (L), selected to ensure the desired interaction "levels" (*i.e.*, $R_{DL}=P_{crD}/P_{crL}$ values), (ii) their critical local and distortional critical buckling loads (E=210GPa, ν=0.3) and (iii) the corresponding buckling mode half-wave numbers (n_D and n_L).

Fig. 1 shows the GBT nodal discretization adopted for both cross-sections, involving three intermediate nodes per wall, and the deformation modes of the column with $P_{crL}\cong P_{crD}$ – note that such a fine discretization is only required for the geometrically non-linear analyses with imperfections (GNIA) conducted in Section 3 (naturally, a less refined nodal discretization suffices in linear buckling analyses). This discretization leads to (i) 41 conventional modes (4 global, 7 distortional and 30 local) – modes **1-41** (see Fig. 1(a)), (ii) 39 shear modes (9 global and 30 local) – modes **42-80** (see Fig. 1(b)), (iii) 40 linear transverse extension modes (1 global isotropic, 7 global deviatoric, 2 distortional and 30 local) – modes **81-120** (see Fig. 1(c)) and (iv) 40 quadratic transverse extension modes (omitted in this figure), totaling 160 (sequentially numbered) deformation modes. On the other hand, Figs. 2(a)-(b) display (i) the critical buckling mode shapes (local and/or distortional) associated with all the initial geometrical imperfections considered in the GBT-based GNIA (discussed in Section 3), (ii) the corresponding GBT modal amplitude functions and (iii) a representative sample of deformed cross-sections located at mid-span or in its close vicinity (Fig. 2(a_3)). In the column undergoing "true L-D interaction", the shapes of the duplicate distortional modes and "single" local modes[5] are adopted as initial geometric imperfections. Naturally, since the purpose of the R_{DL}=2.5 column analyses is to illustrate the emergence of (dominant) distortional deformations at advanced loading stages, only local critical-mode initial geometrical imperfections are considered. Lastly, as shown by Gonçalves & Camotim (2013a), a single (Fig. 2(a_3)+(b)) or a pair (Fig. 2(a_1)+(a_2)) of deformation modes often provide the buckling problem solution.

[4] Columns with $P_{crD}/P_{crL}<1$ (prone to "secondary-local bifurcation L-D interaction") are not analyzed here, since their post-buckling behavior is very similar to that of columns undergoing a "pure" distortional post-buckling behavior. Indeed, the highly dominant role played by the distortional deformations precludes the development of local deformations akin to the critical local buckling mode. This is clearly the least relevant L-D interaction type, since it is associated with negligible strength erosion.

[5] To facilitate the comparison between GBT and ABAQUS shell finite element (SFE) results, even-sided RCPS columns were selected, as they exhibit single local critical buckling modes (for odd-sided RCPS duplicate buckling modes are obtained). Concerning the critical distortional buckling modes, duplicate modes are always obtained for RCPS with more than four walls.

Table 1: Selected RCPS column geometries, buckling loads and critical half-wave numbers (*mm* and *kN*).

n	b	R	t	L	P_{crD}	n_D	P_{crL}	n_L	R_{DL}
10	29.66	54	2.00	350.0	2043.3	1	1881.7	12	1.08
10	33.37	54	1.27	350.0	1165.7	1	467.3	11	2.50

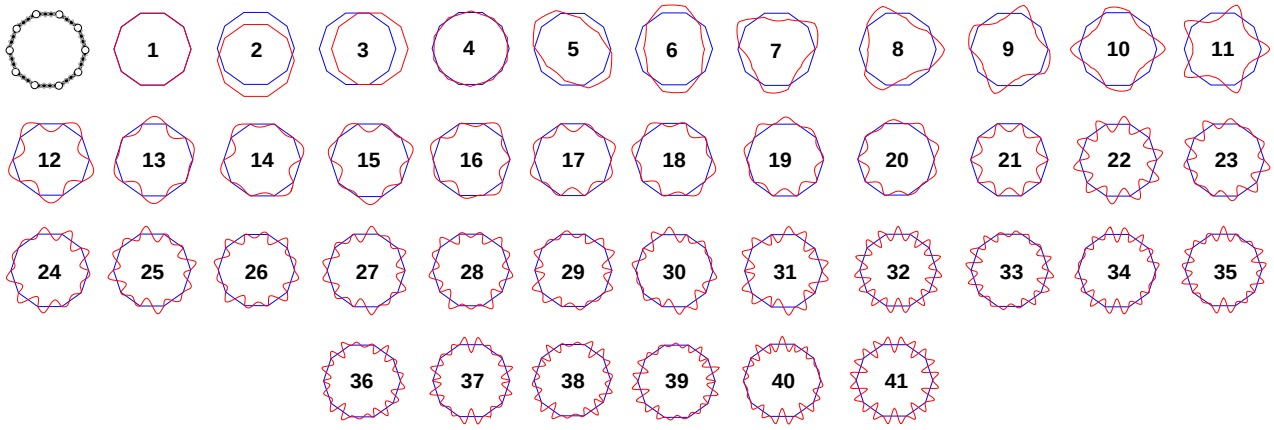

(a)

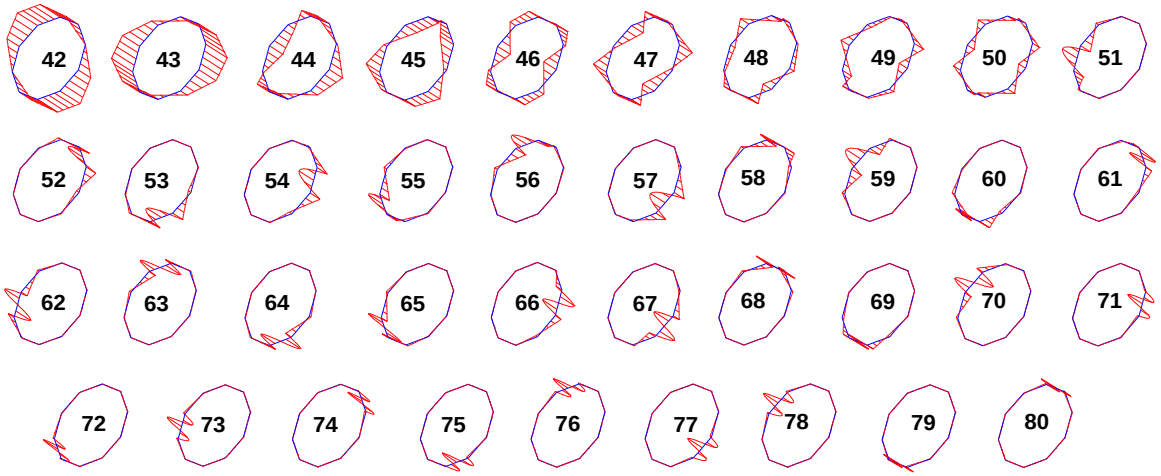

(b)

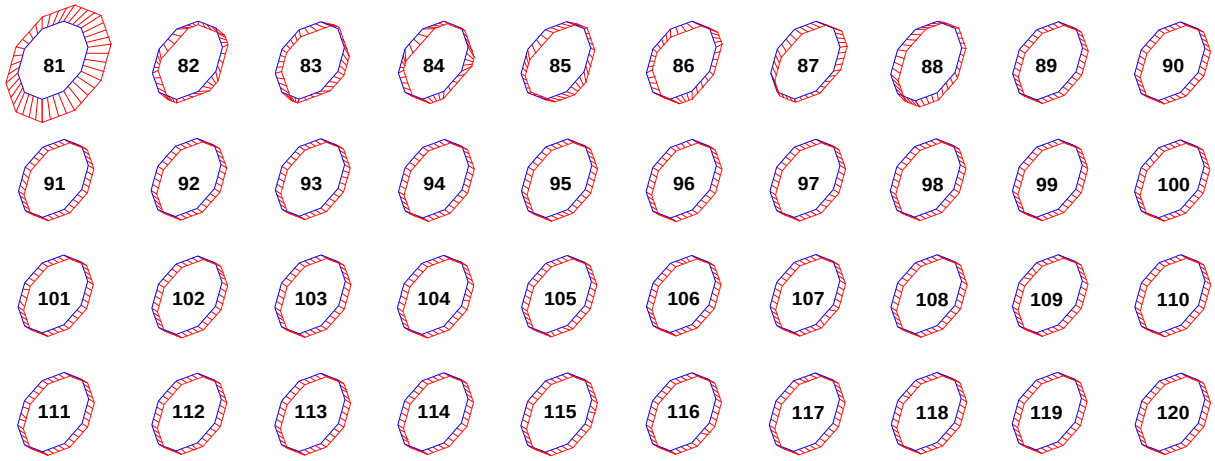

(c)

Figure 1: n=10 RCPS column with $P_{crD}/P_{crL}\cong$1.0 (a) GBT discretization and conventional deformation modes, (b) shear mode warping displacement profiles and (c) linear transverse extension deformation modes.

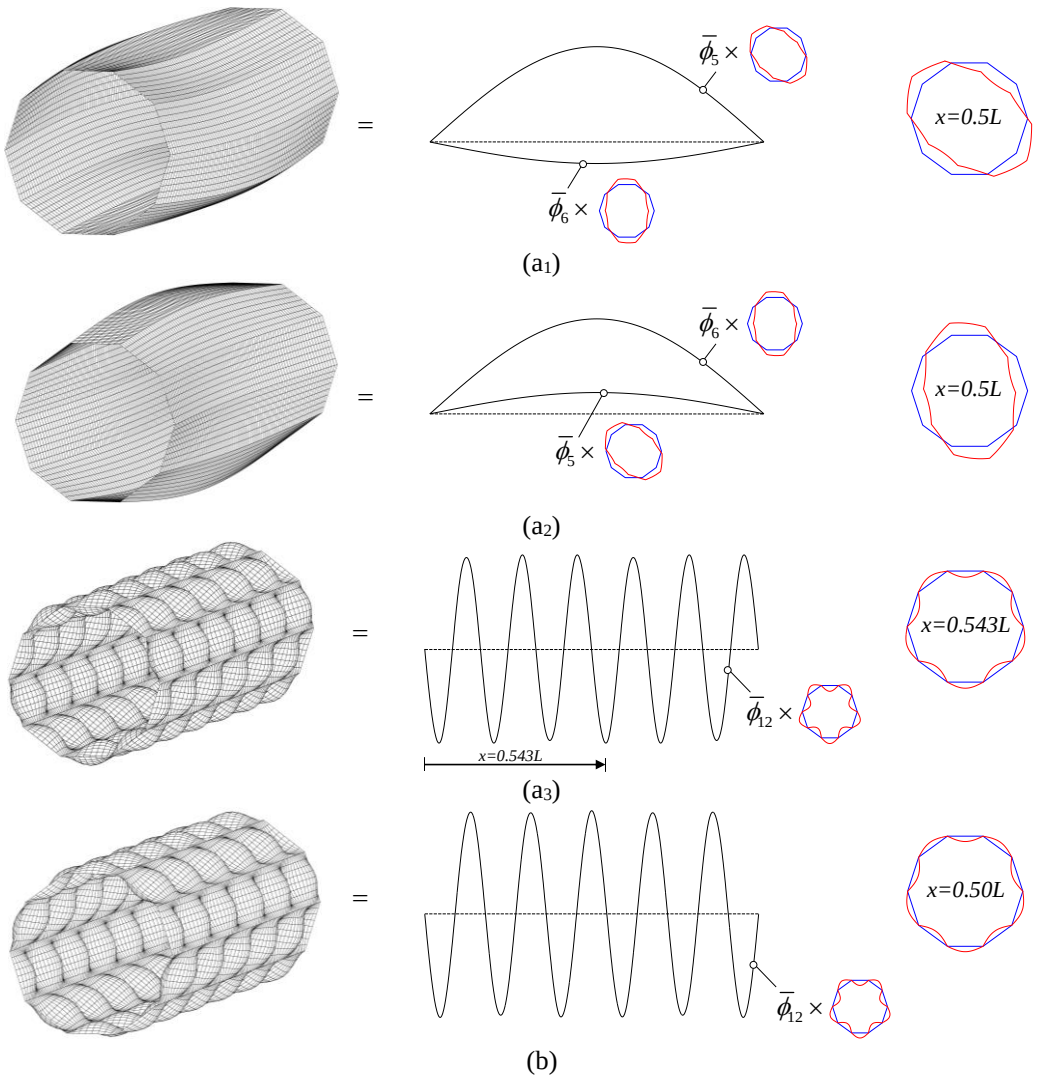

Figure 2: Critical distortional and/or local buckling mode shapes, and associated GBT modal amplitude functions, for n=10 RCPS columns with (a) $P_{crD}/P_{crL} \cong 1.0$ – (1)+(2) correspond to duplicate modes – and (b) $P_{crD}/P_{crL} = 2.5$.

3. Post-Buckling Behavior of Columns Experiencing L-D Interaction

3.1 True L-D interaction

The column analyzed in this section exhibits a critical distortional-to-local buckling load ratio close to one (see Table 1) and, therefore, its post-buckling behavior is expected to be strongly affected by L-D interaction. As mentioned in Section 2, three distinct critical-mode shapes/configurations are adopted as initial geometrical imperfections: one akin to the local critical buckling mode (Fig. 2(a3)) and two akin to the distortional critical buckling modes (Fig. 2(a1)+(a2)) – the corresponding results are discussed in Sections 3.1.1 and 3.1.2, respectively. Each column contains initial geometrical imperfections with four amplitudes (values of the maximum cross-section in-plane displacement), namely 0.5, 0.2, 0.1 and 0.01mm. In addition, an initial geometrical imperfection combining (i) the local critical mode shape, with a 0.5mm amplitude, and (ii) the distortional critical-mode 1 (Fig. 2(a1)), with a 0.01mm amplitude, is also considered, in order to shed new light and clarify a surprising behavioral feature exhibited by the columns containing pure local critical-mode initial imperfections – this issue is addressed in Section 3.1.3.

3.1.1 Local initial geometrical imperfections

Fig. 3(a) shows column equilibrium paths P/P_{cr} vs. $|w|/t$, where w is the flexural displacement at the mid-point of the bottom wall located at $x/L\cong0.543$ caused by the applied axial load P, concerning the columns with the 0.5, 0.2, 0.1 and 0.01mm initial geometrical imperfections – the results presented in this sub-section were obtained with 20 equally-spaced finite elements combined with an arc-length control strategy. On the other hand, Fig. 3(b) shows (i) again the 0.2mm imperfection column equilibrium path (already shown in Fig. 3(a), but with a different horizontal scale), now termed "trivial" (as discussed below), (ii) the corresponding ABAQUS SFEA results and (iii) two "non-trivial" paths (also discussed below) – this column is hereafter termed "$P_{crD}/P_{crL}\cong1.0+L_{0.2mm}$". As for Figs. 4(a)-(c), they show the modal participation diagrams based on the amplitude functions, which quantify the relative importance of each deformation mode (or mode set) along the three $P_{crD}/P_{crL}\cong1.0+L_{0.2mm}$ equilibrium paths, plotted as function of (i) P/P_{cr} (trivial path – Fig. 4(a)), (ii) $|(w+w_0)|/t$ (non-trivial 1 path – Fig. 4(b)) or (iii) $(w+w_0)/t$ (non-trivial 2 path – Fig. 4(c)). Figs. 5(a)-(c) provide the evolution of the $P_{crD}/P_{crL}\cong1.0+L_{0.2mm}$ column modal contributions to the transverse displacement profile of the bottom wall mid-point along the "trivial" equilibrium path of Fig. 3(b), namely the contributions from the (i) local modes ($w_{12\text{-}41}(x)$), (ii) linear transverse extension modes ($w_{81\text{-}120}(x)$) and (iii) all the modes ($w_{1\text{-}160}(x)\equiv w(x)$). Similarly, Figs. 6(a)-(h) and Figs. 7(a)-(h) show the same type of results along the "non-trivial 1" and "non-trivial 2" equilibrium paths of Fig. 3(b), respectively – in this case, more contributions to the bottom wall mid-point transverse displacement profile are depicted, namely those stemming from the (i) major-axis flexural mode **2** ($w_2(x)$), (ii) dominant distortional mode **6** ($w_6(x)$), (iii) less relevant distortional modes **5**, **7**, **8**, **9**, **10**, **11** ($w_{5+7\text{-}11}(x)$),

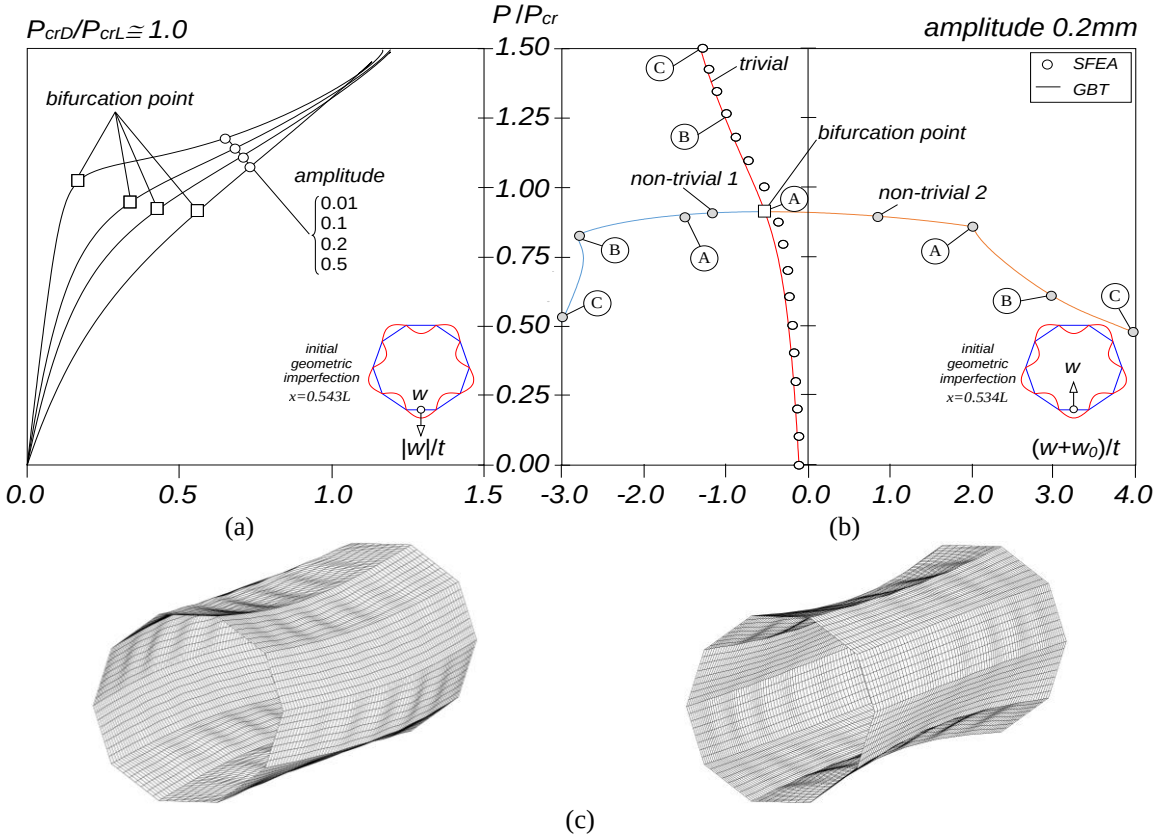

Figure 3: $P_{crD}/P_{crL}\cong1.0+L$ column (a) trivial post-buckling equilibrium paths associated with initial imperfection amplitudes 0.5, 0.2, 0.1, 0.01mm, (b) trivial and two non-trivial equilibrium paths concerning the initial imperfection amplitude 0.2mm, and (c) eigenvectors associated with the negative eigenvalues in the vicinity of the bifurcation point (amplified 3 times).

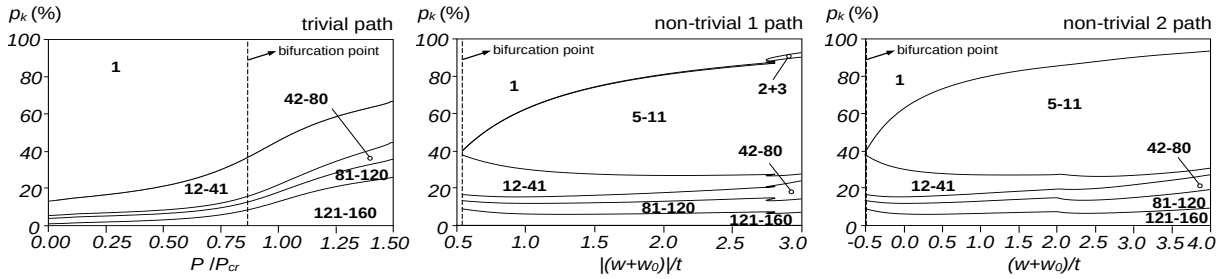

Figure 4: $P_{crD}/P_{crL}\cong 1.0+L_{0.2mm}$ column modal participation diagrams of the (a) trivial (b) non-trivial 1 and (c) non-trivial 2 paths.

(iv) local modes **12-41** ($w_{12\text{-}41}(x)$), (v) linear transverse extension modes **81-120** ($w_{81\text{-}120}(x)$) and (vi) all the modes ($w_{1\text{-}160}(x)\equiv w(x)$) – note that the symbol ($^{\downarrow}$) appearing in these figures, identifies an equilibrium point located on the descending branch, *i.e.*, beyond the limit point. Finally, Figs. 8(a_1)-(c_3) show GBT deformed configurations at equilibrium states located on the $P_{crD}/P_{crL}\cong 1.0+L_{0.2mm}$ column equilibrium paths (see Fig. 3(b)) – three states per equilibrium path (states "A", "B" and "C"). The observation of all these GBT post-buckling results leads to the following conclusions:

(i) Fig. 3(a) shows that, in all the columns analyzed (same geometry and identical initial imperfections with distinct amplitudes), the equilibrium paths always exhibit a significantly high post-critical strength. Moreover, the close observation of the associated longitudinal displacement profiles of the $P_{crD}/P_{crL}\cong 1.0+L_{0.2mm}$ column (displayed in Figs. 5(a)-(c)), together with the deformed configurations depicted in Figs. 8(a_1)-(a_3), readily shows that such high-strength equilibrium paths are those typical of a local post-buckling behavior (*e.g.*, Martins *et al*. 2018a). Indeed, there is a strong resemblance between the displacement profiles shown in Figs. 5(a)-(c) and those reported recently for even-sided RCPS columns with a typical/"pure" local post-buckling behavior (Martins *et al*. 2018a). This means that these columns do not experience L-D interaction, which is very surprising given the closeness between the critical local and distortional buckling loads – such behavioral feature has never been observed in the context of open (lipped) cross-section columns (*e.g.*, Martins *et al*. 2015, 2018b) or any other coupling phenomenon (*e.g.*, Camotim *et al*. 2018). In particular, there is no trace of distortional deformations, as attested by the absence of such deformations in the modal participation diagram shown in Fig. 4(a) – rigorously speaking, the comparison between this modal participation diagram, concerning n=10 columns, and that reported by Martins *et al*. (2018a) for n=4 columns shows (i_1) larger participations from mode **1** and the transverse extension modes, and (i_2) smaller local mode contributions at advanced loading stages ($1.00<P/P_{cr}<1.50$).

(ii) Since the GBT solutions, validated by the ABAQUS SFEA results (see Fig. 3(b)), are quite surprising (absence of L-D interaction), eigenvalue analyses of the GBT global tangent stiffness matrix were conducted at each equilibrium point. It was found that two negative eigenvalues appear in the close vicinity of the critical bifurcation load level (recall that $P_{crL}\cong P_{crD}$), which indicates loss of uniqueness of the numerical solution – the corresponding equilibrium states are identified by white squares in Fig. 3(a) and termed "bifurcation points". Rigorously speaking, the location of the bifurcation points depends mildly on the initial imperfection amplitude, since they occur at lower loading levels as the initial imperfection amplitude increases – for instance, the bifurcation point locations for the 0.01 and 0.5mm columns are P/P_{cr}=0.914 and P/P_{cr}=1.022, respectively. Therefore, multiple equilibrium paths branch out from these equilibrium states: one "trivial" (already addressed in Fig. 3(a)) and two "non-trivial", depicted in Fig. 3(b) for the $P_{crD}/P_{crL}\cong 1.0+L_{0.2mm}$ column – the latter are obtained through an *eigenvector injection* into the first iteration of the incremental procedure, in the vicinity of the anticipated bifurcation point, as described in, for instance, in Borst *et al*. (2012). Moreover,

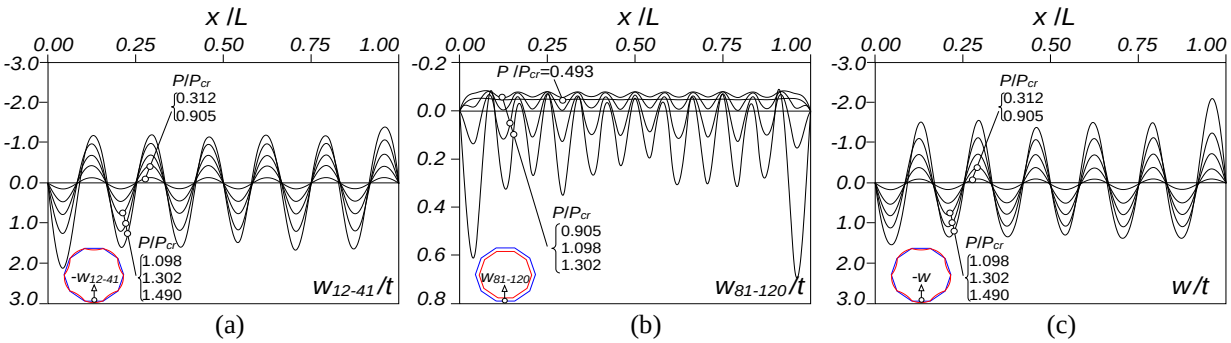

Figure 5: $P_{crD}/P_{crL} \cong 1.0+L_{0.2mm}$ column displacement profiles (a) $w_{12\text{-}41}(x)$, (b) $w_{81\text{-}120}(x)$ and (c) $w_{1\text{-}160}(x) \equiv w(x)$ along the trivial equilibrium path.

any linear combination of the two eigenvectors displayed in Fig. 3(c) provides additional non-trivial solutions. However, the non-trivial solutions considered in this work are always searched in the direction of one of the two eigenvectors, *i.e.*, the non-trivial 1 and 2 equilibrium paths in Fig. 3(b) correspond to the injections of eigenvector 1 or 2, respectively associated with the first and second negative eigenvalues. It should be stressed that, to the authors' best knowledge, no branch switching techniques are implemented in the ABAQUS SFEA, which implies that no comparison can be made with the GBT non-trivial solutions[6]. However, it is worth noting that two negative eigenvalues were also detected, near the bifurcation load level, in equilibrium points obtained by ABAQUS SFEA[7].

(iii) The observation of the "non-trivial" modal participation diagrams (Fig. 4(b)-(c)) (iii_1) unveils the emergence of distortional deformations immediately after the bifurcation point, which rapidly become the major source of the deformation taking place in the two alternative/secondary paths, mostly due to a reduction of the contributions from mode **1** and the local modes, and (iii_2) shows how much these non-trivial paths differ from the trivial one – naturally, this distortional deformation dominance prompts the occurrence of L-D interaction in the two alternative paths (as discussed further in item (iv)). For instance, the participation of the distortional modes (mostly modes **5** and **6**) reaches maximums of 62.8% and 63.5% at $|(w+w_0)|/t=2.981$ ($P/P_{cr}=0.534^{\downarrow}$) and $(w+w_0)/t=3.392$ ($P/P_{cr}=0.548^{\downarrow}$), respectively for the non-trivial paths 1 and 2. The local mode contributions gradually decrease along the two non-trivial paths from 21.2% to 3.7% ("non-trivial 1") and 21.5% to 3.5% ("non-trivial 2"). Conversely, it is observed that the joint participation of all shear modes significantly increase from 3.2% to 9.6% ("non-trivial 1") and 3.1% to 7.9% ("non-trivial 2"). Moreover, the joint participation of the linear and quadratic transverse extension modes changes only a little along the two equilibrium paths (it varies between 12% and 19%).

(iv) The analysis of the displacement profiles shown in Figs. 6(a)-(f) and 7(a)-(f), concerning the "non-trivial 1" and "non-trivial 2" equilibrium paths, confirms that these columns undergo L-D interaction – the deformed configurations displayed in Figs. 8(b_1)-(c_3) further reinforce this assertion. As mentioned in the previous item, distortional deformations develop immediately after the bifurcation point, particularly those associated with mode **6** (see Figs. 6(b) and 7(b)), exhibiting a single half-wave, akin to the critical distortional buckling mode, and retain this shape along the whole smooth descending path[8], *i.e.*, until equilibrium states "B" and "A" are reached (see Fig. 3(b)), respectively

[6] Rigorously speaking, it was possible to compute a non-trivial solution with ABAQUS SFEA in one case (see Section 3.1.2).

[7] This information can be retrieved from the .msg output file generated during the execution of ABAQUS analysis.

[8] The slight negative concavity in the close vicinity of the bifurcation load level also (indirectly) attests the occurrence of L-D interaction – this feature characterizes the RCPS column distortional post-buckling behavior (see Martins *et al.* 2018a).

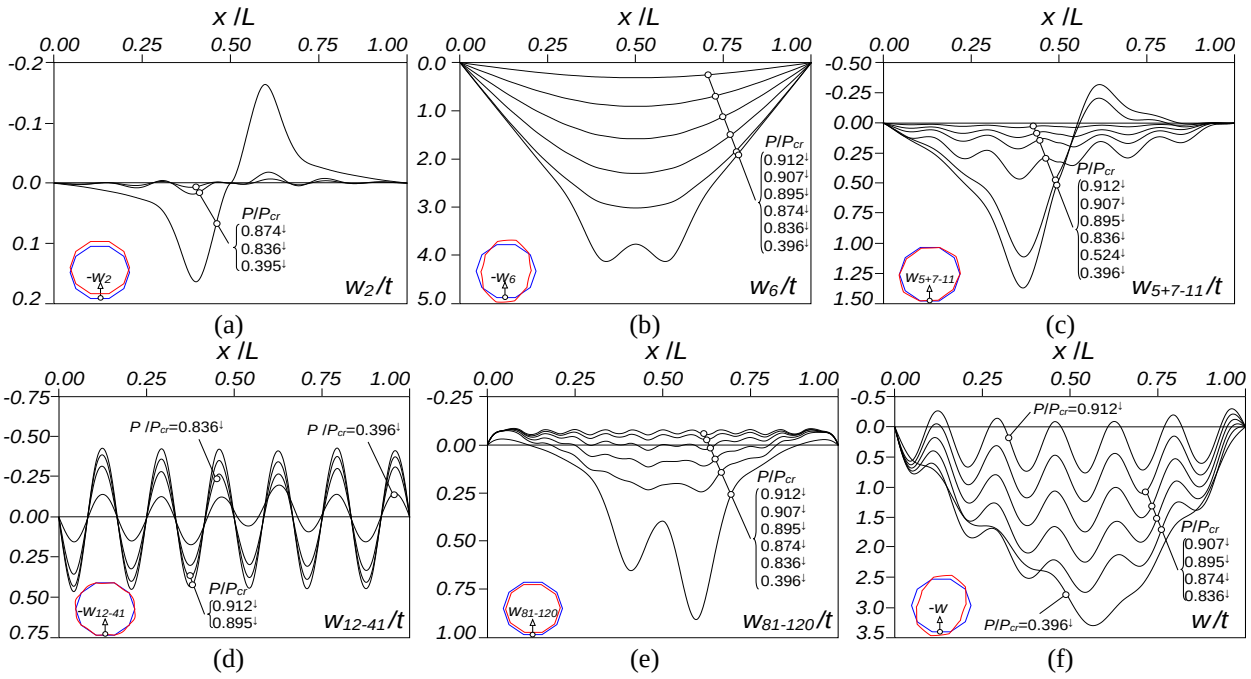

Figure 6: $P_{crD}/P_{crL}\cong 1.0+L_{0.2mm}$ column displacement profiles (a) $w_2(x)$, (b) $w_6(x)$, (c) $w_{5+7-11}(x)$, (d) $w_{12-41}(x)$, (e) $w_{81-120}(x)$, and (f) $w_{1-160}(x)\equiv w(x)$ – non-trivial 1 path.

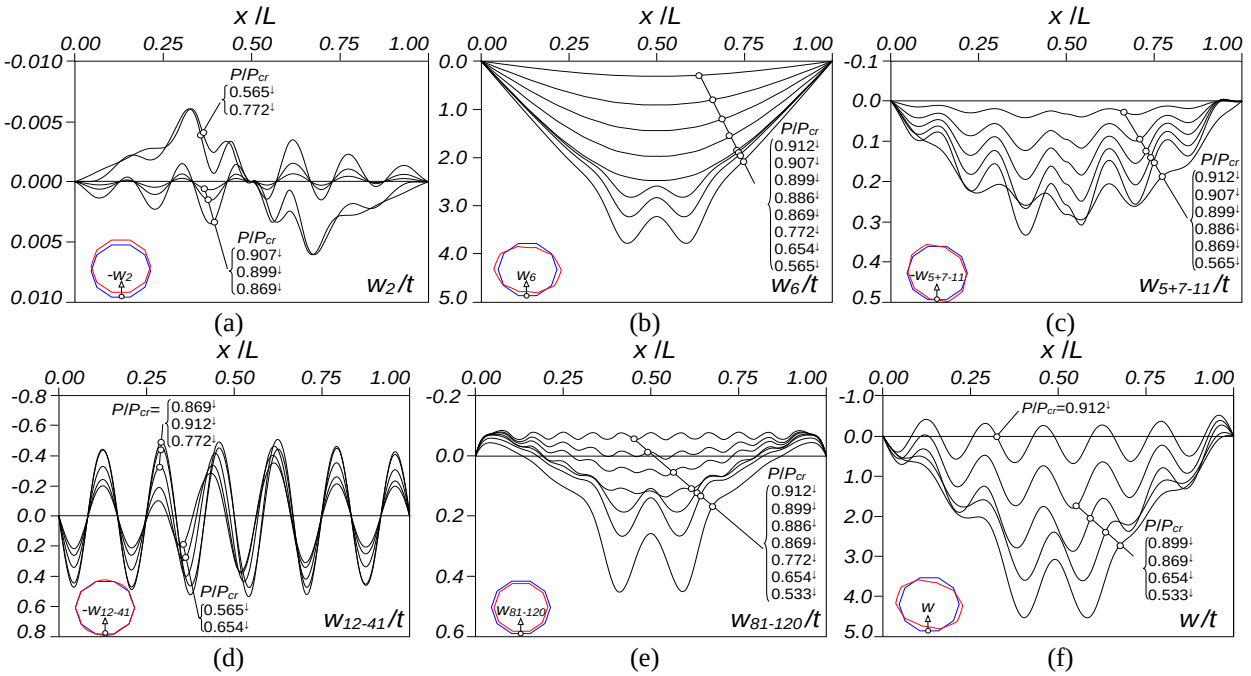

Figure 7: $P_{crD}/P_{crL}\cong 1.0+L_{0.2mm}$ column displacement profiles (a) $w_2(x)$, (b) $w_6(x)$, (c) $w_{5+7-11}(x)$, (d) $w_{12-41}(x)$, (e) $w_{81-120}(x)$, and (f) $w_{1-160}(x)\equiv w(x)$ – non-trivial 2 path.

for the "non-trivial 1" and "non-trivial 2" paths, thus constituting a very clear sign of the occurrence of coupling between local and distortional buckling – recall that local deformations also take place along those equilibrium paths via the initial geometrical imperfections. At more advanced stages (*i.e.*, beyond points "A" and "B"), the distortional deformation patterns gradually change from one half-wave to three small "local buckles" in the mid-span regions – this local phenomenon occurs in

all the columns analyzed (2 non-trivial paths and 4 initial geometrical amplitudes). Moreover, it is still worth noting that the dominant distortional mode **6** has opposite contributions in the two non-trivial equilibrium paths, regardless of the initial imperfection amplitude considered.

(v) The non-trivial equilibrium paths are the most relevant, since they exhibit significant strength and stiffness erosion with respect to the trivial one, which is due to the L-D interaction effects. This clearly shows that this coupling phenomenon must be taken into account in design provisions. This issue will be further addressed in Section 3.1.3, where the trivial equilibrium path of an initially imperfect column, whose imperfection consists of a linear combination of critical local and distortional buckling mode shapes, is determined and briefly discussed.

(vi) Turning now the attention to the local longitudinal displacement profiles concerning the non-trivial 2 equilibrium path (Fig. 7(d)), it can be readily concluded that $w_{12\text{-}41}(x)$, initially exhibiting 12 equal half-waves, retains its configuration and amplitude up to P/P_{cr}=0.854$^{\downarrow}$ (state "A" in Fig. 3(b)). At more advanced post-buckling stages, it begins to change gradually, to exhibit a central half-wave ($x/L\cong$0.50) with outward motions and two adjacent half-waves with inward motions[9] (like the dominant pattern $w_6(x)$), which is combined with a slight amplitude reduction – recall $p_{12\text{-}41}$ in Fig. 4(c). Naturally, the displacement profile $w(x)$ tends to exhibit a symmetric configuration at advanced loading stages (*e.g.*, P/P_{cr}=0.533$^{\downarrow}$ in Fig. 7(f)). On the other hand, the $w_{12\text{-}41}(x)$ regarding the non-trivial 1 equilibrium path (Fig. 6(d)) retains its 12 half-waves with quite similar amplitudes up to P/P_{cr}=0.858$^{\downarrow}$ (state "B" in Fig. 3(b)), like in the previous case. As loading progresses, the amplitude decreases with no visible configuration change, unlike in the non-trivial 2 equilibrium path.

(vii) The observation of the displacement profiles (Figs. 6 and 7) and 3D deformed configurations (Figs. 8(b)+(c)) concerning the two non-trivial equilibrium paths shows that both are affected by L-D interaction (as already discussed). However, the nature of the distortional mode involved is different. Indeed, the coupling in the non-trivial 2 path involves major participations from the dominant modes **5**+**6**, *i.e.*, the "trivial" distortional configuration discussed in Martins *et al*. (2018a) (recall the discussion in this paper Introduction). On the other hand, the non-trivial 1 equilibrium path involves, besides the participations of the distortional modes **5**+**6**, significant contributions from the other distortional modes (Fig. 6(c)), flexural modes (Fig. 6(a)) and transverse extension modes (Fig. 6(e)), which lead to the formation of two "kinks" in the mid-span region, particularly visible in Fig. 8(b_3) – the formation of these two "kinks" (instead of one) is due to the even number of local half-waves (n_L) exhibited by the initial imperfection[10]. Note that this behavioral feature is responsible for the asymmetry of the $w(x)$ longitudinal profile (see Fig. 6(f)).

(viii) A direct consequence of the content of the two previous items (local and distortional displacement profiles) is the fact that the distortional deformations (mainly consisting of mode **6** in this particular case) strongly influence the L-D interaction mechanics in RCPS columns, like in open-section (lipped) columns (*e.g.*, Martins *et al*. 2018b). Then, it is just natural to expect that the (true) L-D interaction behavior will be governed by distortional deformations. Indeed, there is a strong similarity between the "pure" distortional post-buckling behavior reported by Martins *et al*. (2018a) and that analyzed in this section, associated with true L-D interaction. Although not particularly clear in the non-trivial 1 equilibrium path, the non-dominant deformation pattern in the L-D interaction behavior, (*i.e.*, the local deformations) is strongly influenced by the configuration of the dominant distortional

---

[9] This behavioral feature may cease to occur if the local half-wave number is smaller, since the central half-wave nature becomes more important in relative terms.

[10] Section 3.2 addresses a column containing an initial imperfection with an odd local half-wave number (intentionally chosen).

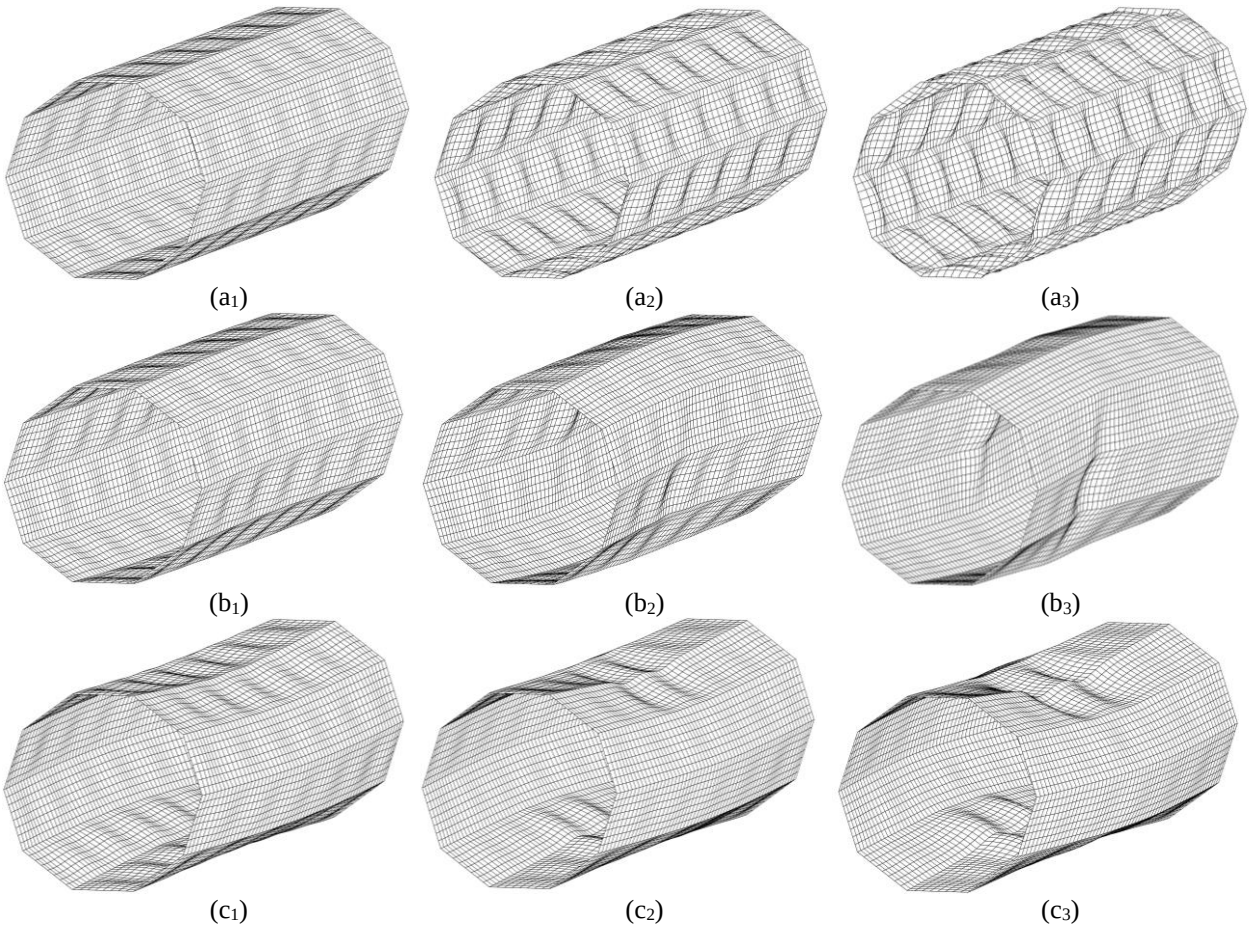

Figure 8: $P_{crD}/P_{crL} \cong 1.0+L_{0.2mm}$ column post-buckling deformed configurations at P/P_{cr} equal to (a_1) 0.905 (bifurcation point), (a_2) 1.255 and (a_3) 1.499 (trivial path), (b_1) $0.902^{\downarrow}$, (b_2) $0.806^{\downarrow}$ and (b_3) $0.524^{\downarrow}$ (non-trivial 1 path), and (c_1) $0.843^{\downarrow}$, (c_2) $0.610^{\downarrow}$ and (c_3) $0.533^{\downarrow}$ (non-trivial 2 path).

deformations – this was clearly visible in the non-trivial 2 equilibrium path. Such behavioral feature is more pronounced in columns with higher critical distortional-to-local buckling load ratios, like the one analyzed in Section 3.2. This implies that a significant difference between the local displacement profiles of columns containing critical-mode (local) initial geometrical imperfection with distinct amplitudes is to be expected (see discussion below) – note that, although aware of this issue, the authors never assessed this influence in open lipped cross-section columns.

The results presented next concern the $P_{crD}/P_{crL}=1.0+L_{0.01mm}$ column (smallest initial imperfection amplitude considered). Since these results are similar to those just presented, their descriptions are abbreviated whenever possible. Fig. 9(a) shows three P/P_{cr} vs. $(w+w_0)/t$ equilibrium paths (like Fig. 3(b)), while Fig. 9(b_1)+(b_2) displays the modal participation diagrams corresponding to the non-trivial 1 and 2 equilibrium paths, respectively. Lastly, Fig. 10 shows the contributions, to the cross-section transverse displacement $w(x)$, of (i) mode **6** ($w_6(x)$ – dominant distortional mode), (ii) **12-41** ($w_{12\text{-}41}(x)$ – local modes) and (iii) all modes ($w_{1\text{-}160}(x) \equiv w(x)$), along the non-trivial 1 (Fig. 10(a_1)-(c_1)) and 2 (Fig. 10(a_2)-(c_2)) equilibrium paths. The observation of these results makes it possible to conclude that:

(i) The qualitative evolutions of the three equilibrium paths shown in Fig. 9(a) are very similar to those depicted in Fig. 3(b). Moreover, there is a strong resemblance between the modal participation diagrams displayed in Figs. 9(b_1)+(b_2) and 4(c)+(b) – the only perceptible difference is the higher

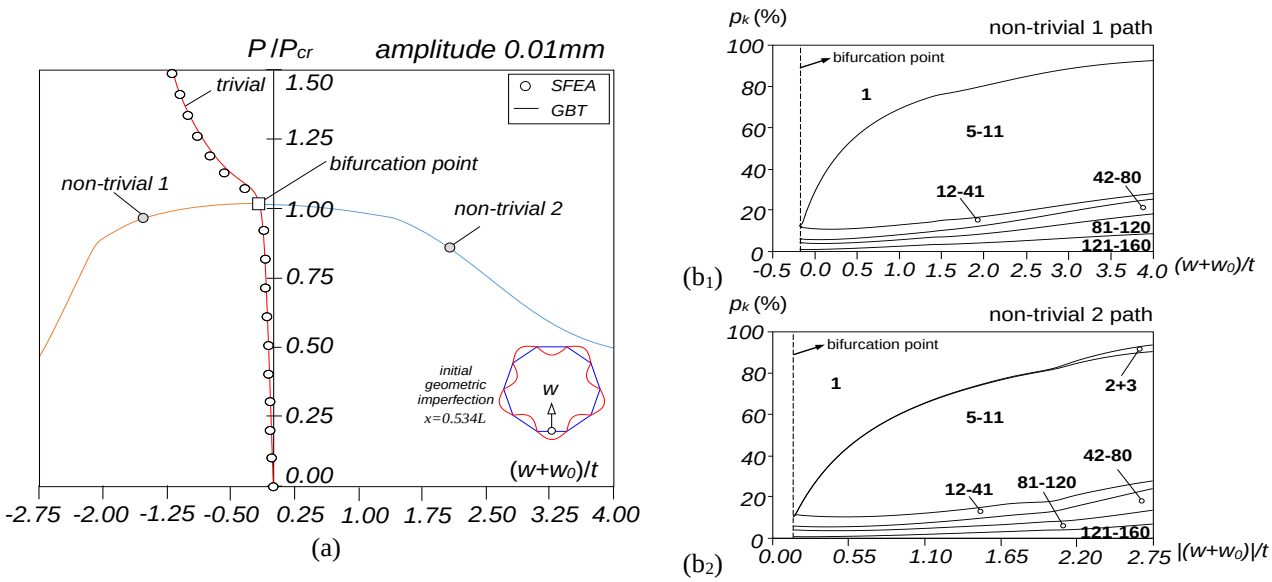

Figure 9: $P_{crD}/P_{crL}\cong 1.0+L_{0.01mm}$ column (a) post-buckling equilibrium paths P/P_{cr} vs. $(w+w_0)/t$ and (b) modal participation diagrams concerning the non-trivial ($_1$) 1 and ($_2$) 2 equilibrium paths.

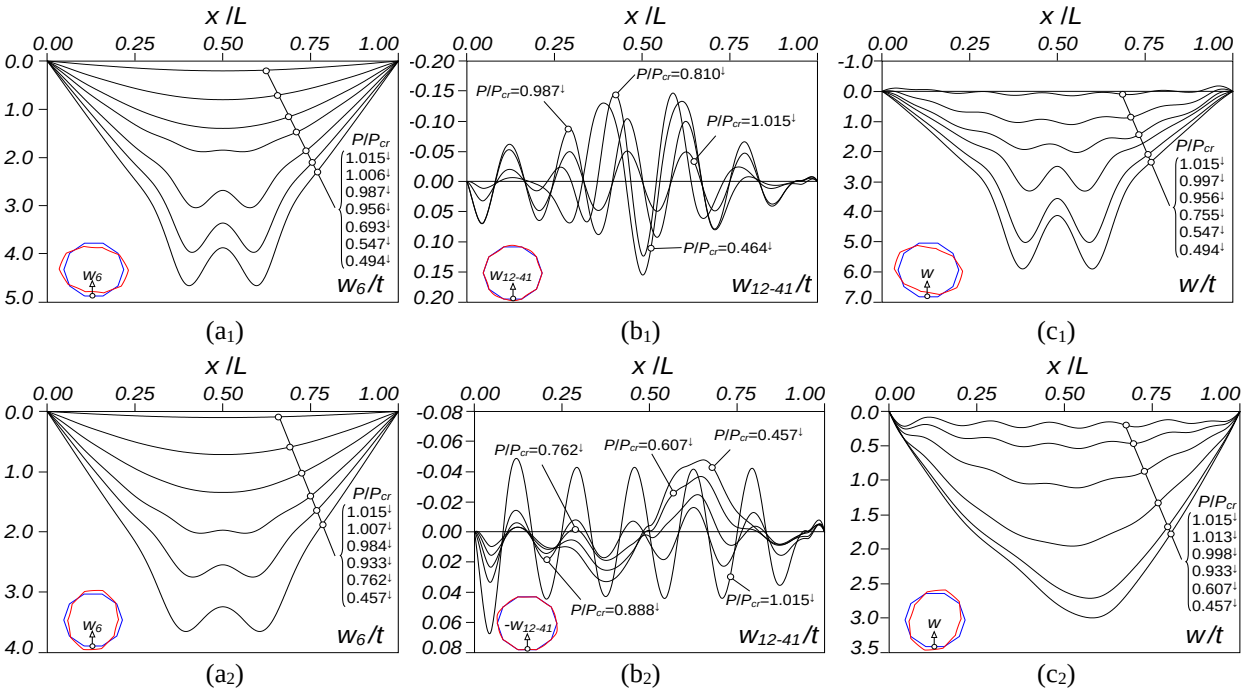

Figure 10: $P_{crD}/P_{crL}\cong 1.0+L_{0.01mm}$ column displacement profiles (a) $w_6(x)$, (b) $w_{12\text{-}41}(x)$ and (c) $w_{1\text{-}160}(x)\equiv w(x)$, concerning the non-trivial ($_1$) 1 and ($_2$) 2 equilibrium paths.

participation of mode **1** in the vicinity of the bifurcation point, which is just logical in view of the much smaller initial geometrical imperfection amplitude considered.

(ii) The dominant longitudinal profiles $w_6(x)$ are very similar to those shown previously in Figs. 6(b) and 7(b). However, as expected, the (non-dominant) local longitudinal profiles $w_{12\text{-}41}(x)$ are very distinct. Indeed, progressing along the non-trivial 1 path, the $w_{12\text{-}41}(x)$ contributions change gradually to exhibit one outward and two inward central half-waves (as the $w_6(x)$ contribution), while some of the remaining half-waves invert their motions – *e.g.*, compare Figs. 10(b$_1$) and 7(d). Recalling that the

non-trivial 2 path exhibits two "kinks" near the mid-span region (at advanced loading stages), note that the $w_{12\text{-}41}(x)$ contribution also changes gradually to exhibit two (wavy) half-waves near mid-span, unlike its $P_{crD}/P_{crL}\cong 1.0+L_{0.2mm}$ column counterpart shown in Fig. 6(d) – naturally, a local "sign" change takes place at the transition. Based on the comparison between the local displacement profiles of these two columns ($L_{0.2mm}$ and $L_{0.01mm}$), it can be concluded that they are significantly affected by the imperfection amplitude when critical local mode initial imperfections (akin to the non-dominant deformations) are employed.

3.1.2 Distortional initial geometrical imperfections

The results addressed in this sub-section are presented similarly to those discussed previously, *i.e.*, they consist of equilibrium paths, modal participation diagrams, modal displacement profiles and 2D/3D deformed configurations. They concern columns with initial geometrical imperfections akin to the (duplicate) critical distortional buckling mode (see Figs. 2(a_1)+(a_2)). All GNIA results were obtained with an arc-length control strategy employing 20 or 30 equally-spaced finite elements. Figs. 11(a)+(b) show several P/P_{cr} vs. $(w+w_0)/t$ trivial/fundamental equilibrium paths (w is shown in the figure and w_0 is its initial value), corresponding to initial imperfections with the shapes of each duplicate critical buckling mode and four amplitudes (0.5, 0.2, 0.1 and 0.01mm). On the other hand, Fig. 12 shows detailed results of the column containing Imperfection 1 with amplitude 0.5mm (hereafter termed $P_{crD}/P_{crL}\cong 1.0+D^1{}_{0.5mm}$), namely (i) three equilibrium paths (Fig. 12(a)), (ii) two buckling modes (Fig. 12(b) – discussed below) and (iii) modal participation diagrams regarding the three equilibrium paths (Figs. 12(c_1)-(c_3)). Figs. 13-15 provide the evolution of the $P_{crD}/P_{crL}\cong 1.0+D^1{}_{0.5mm}$ column modal contributions to the bottom wall mid-point transverse displacement profile for each equilibrium path displayed in Fig. 12(a), namely the contributions of (i_1) the (dominant) distortional mode **6** ($w_6(x)$), (i_2) the (less relevant) distortional modes **5**, **7**, **8**, **9**, **10** and **11** ($w_{5+7\text{-}11}(x)$), (i_3) the local modes **12-41** ($w_{12\text{-}41}(x)$), (i_4) the linear transverse extension modes **81-120** ($w_{81\text{-}120}(x)$) and (i_5) all the modes ($w_{1\text{-}160}(x)\equiv w(x)$) – Figs. 13(a)-(e) and 14(a)-(e) –, and from (ii_1) the major and minor-axis flexural modes **2**+**3** ($w_{2+3}(x)$), (i_2) the (dominant) distortional modes **5** and **6** ($w_{5+6}(x)$), (i_3) the (less relevant) distortional modes **7**, **8**, **9**, **10** and **11** ($w_{7\text{-}11}(x)$), (i_4) the local modes **12-41** ($w_{12\text{-}41}(x)$), (i_5) the linear transverse extension modes **81-120** ($w_{81\text{-}120}(x)$) and (i_6) all the modes

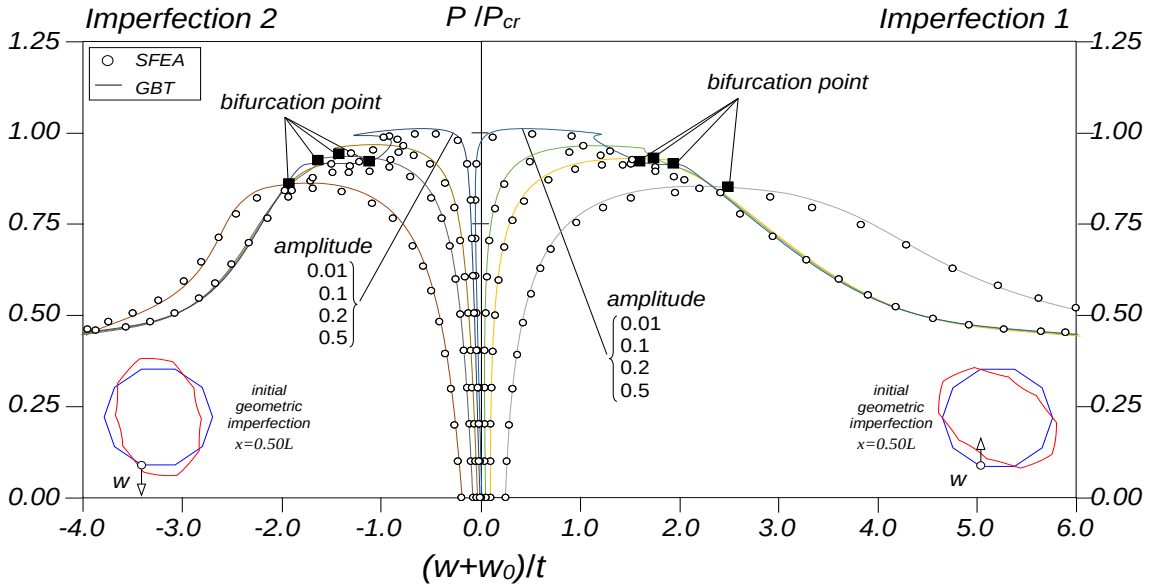

Figure 11: $P_{crD}/P_{crL}\cong 1.0+D$ column post-buckling equilibrium paths associated with two critical-mode initial geometrical imperfections and several amplitudes.

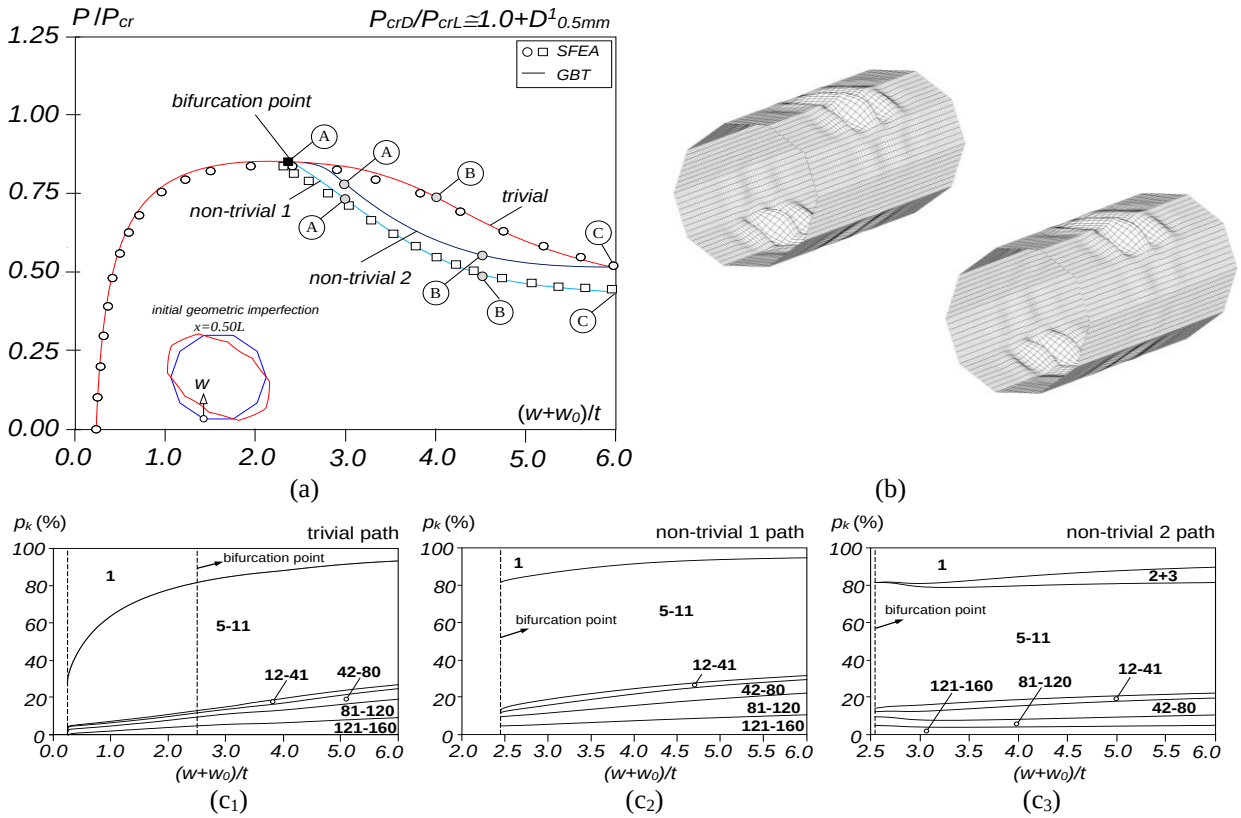

Figure 12: $P_{crD}/P_{crL}\cong 1.0+D^{1}_{0.5mm}$ column (a) post-buckling equilibrium paths P/P_{cr} vs. $(w+w_0)/t$, (b) buckling modes, and (c) modal participation diagrams concerning the $(_1)$ trivial, $(_2)$ non-trivial 1 and $(_3)$ non-trivial 2 equilibrium paths.

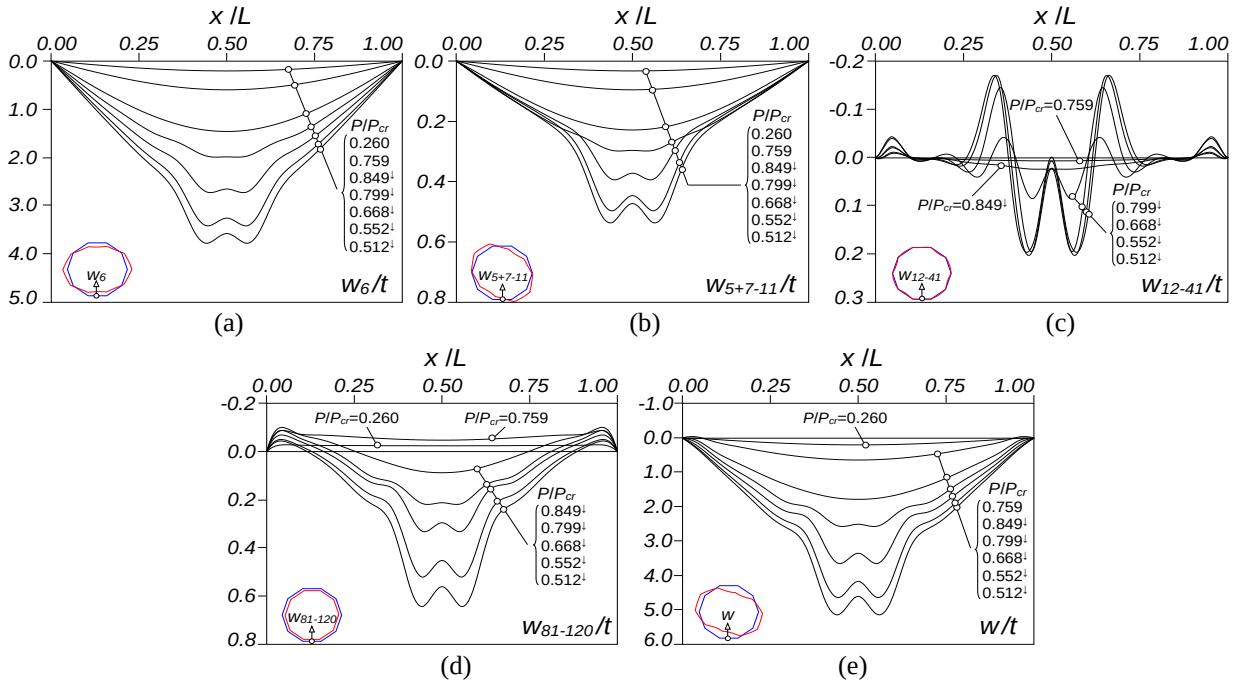

Figure 13: $P_{crD}/P_{crL}\cong 1.0+D^{1}_{0.5mm}$ column displacement profiles (a) $w_6(x)$, (b) $w_{5+7-11}(x)$, (c) $w_{12-41}(x)$, (d) $w_{81-120}(x)$, and (e) $w_{1-160}(x)\equiv w(x)$ – trivial path.

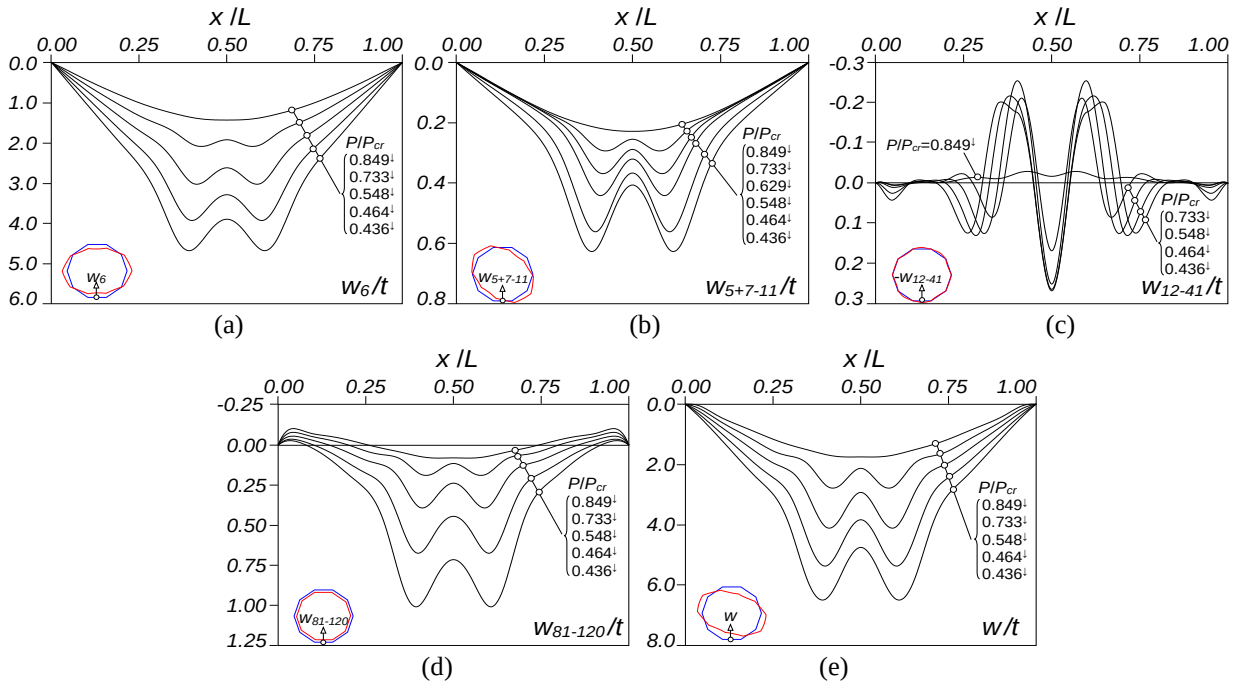

Figure 14: $P_{crD}/P_{crL}\cong 1.0+D^{1}_{0.5mm}$ column displacement profiles (a) $w_6(x)$, (b) $w_{5+7-11}(x)$, (c) $w_{12-41}(x)$, (d) $w_{81-120}(x)$, and (e) $w_{1-160}(x)\equiv w(x)$ – non-trivial 1 path.

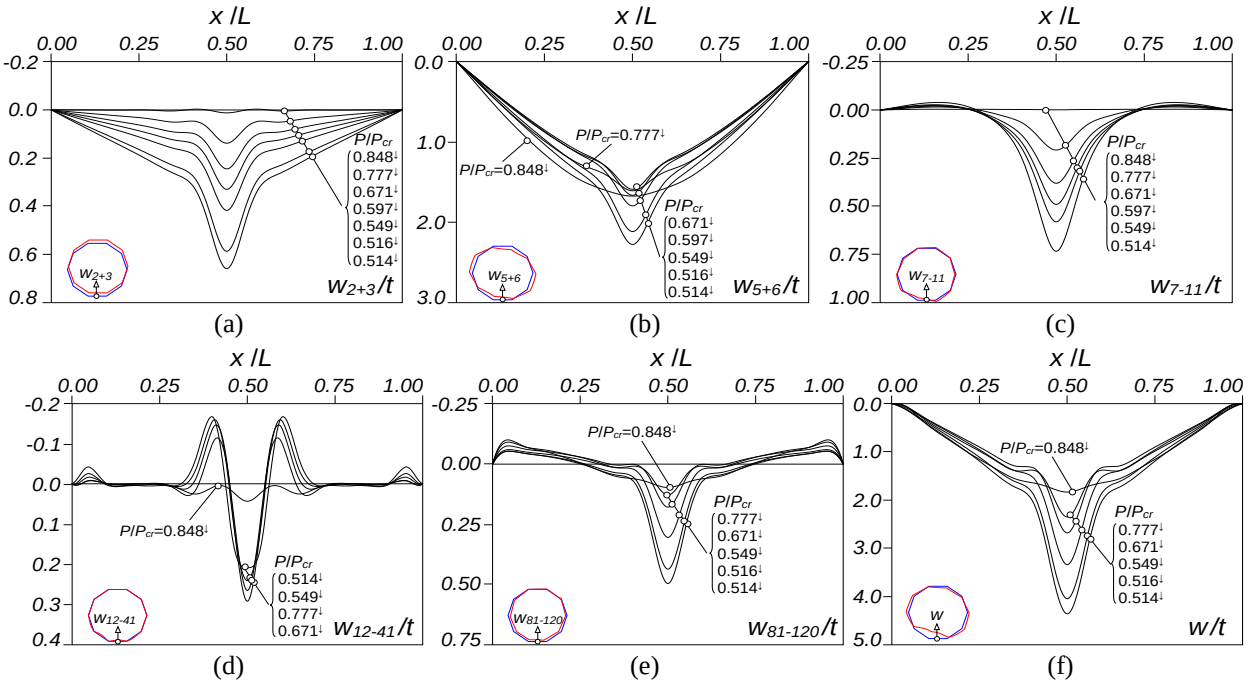

Figure 15: $P_{crD}/P_{crL}\cong 1.0+D^{1}_{0.5mm}$ column displacement profiles (a) $w_{2+3}(x)$, (b) $w_{5+6}(x)$, (c) $w_{7-11}(x)$, (d) $w_{12-41}(x)$, (e) $w_{81-120}(x)$, and (f) $w_{1-160}(x)\equiv w(x)$ – non-trivial 2 path.

($w_{1-160}(x)\equiv w(x)$) – Figs. 15(a)-(f). Finally, Figs. 16(a_1)-(c_3) show GBT-based deformed configurations concerning equilibrium states ("A", "B" and "C") located on the three equilibrium paths of Fig. 12(a). The observation of all these GBT post-buckling results leads to the following conclusions:

(i) First of all, there is an excellent agreement between the results obtained with GBT and the refined S4 ABAQUS SFEA (see Fig. 11). Note that, unlike in the previous case (local critical-mode initial geometrical imperfection with an even half-wave number), the comparison between the two analyses (GBT vs. SFEA) is far from trivial, due to the duplicity of the distortional buckling modes, which define a 2D distortional buckling mode space. In order to make the analyses comparable, it was necessary to combine the two SFEA distortional buckling modes and determine the "rotation" (in the 2D buckling mode space) needed to match the distortional imperfection specified in the GBT analyses – see Martins *et al*. (2018a).

(ii) The column maximum load is significantly affected by (distortional) initial geometrical imperfection amplitude, but not by its shape (or "rotation" in the 2D buckling mode space). Indeed, only the columns with very small initial imperfection amplitudes (*e.g.*, 0.01mm) can reach loads close to the perfect columns bifurcation load. Higher amplitudes, such as 0.5mm, lead to a 15% ultimate strength decrease. These observations are very similar to those reported by Martins *et al*. (2018a) regarding the pure distortional post-buckling behavior of RCPS columns.

(iii) As for the columns analyzed in the previous sub-section, the solution with these initial conditions is also not unique, since eigenvalue analyses of the global tangent stiffness matrix along the trivial equilibrium path descending branch unveil negative eigenvalues. The columns with 0.5mm initial imperfection ($D^1_{0.5mm}$ and $D^2_{0.5mm}$) exhibit two new negative eigenvalues (besides that associated with the trivial path descending branch), while only one is detected in the other columns. The equilibrium states where these negative eigenvalues exist are indicated in Fig. 11 and termed "bifurcation points" – they occur at larger displacements as the initial geometrical imperfection amplitude increases.

(iv) In the particular case of the $P_{crD}/P_{crL}\cong 1.0+D^1_{0.5mm}$ column (Figs. 12-16), two non-trivial solutions are obtained through the injection of the eigenvectors associated with the new negative eigenvalues referred in the previous item, which correspond to the equilibrium paths denoted as "non-trivial 1" and "non-trivial 2", displayed in Fig. 12(a) – note that, unlike in the previous sub-sections, it is possible to obtain one ABAQUS SFEA non-trivial equilibrium path matching the GBT "non-trivial 2" one (the square dots in Fig. 12(a))[11]. As was mentioned in the previous Sub-section, any linear combination of the two eigenvectors, represented in Fig. 12(b), is also a potential solution, contrarily to the $D^1_{0.2mm}$, $D^1_{0.1mm}$, $D^1_{0.01mm}$, $D^2_{0.2mm}$, $D^2_{0.1mm}$, $D^2_{0.01mm}$ columns, where there is only one non-trivial solution. A brief analysis of the content of Figs. 12-16 shows that the behavioral features of the trivial and non-trivial 1 equilibrium paths are very similar, therefore the conclusions/observations for these two cases are presented jointly (items (v) and (vi)).

(v) As was expected, the trivial solution exhibits dominant distortional patterns along the equilibrium path (mostly due to modes **5**+**6**, with a minor contribution from mode **9**) – the exception concerns the early loading stages, where the contribution of mode **1** is prevalent (see Fig. 12(c_1)). For instance, in the vicinity of the bifurcation point, one has: p_1=18.5%, $p_{5\text{-}11}$=68.6% (p_5=40.6% and p_6=26.7%), $p_{12\text{-}41}$=1.3%, $p_{42\text{-}80}$=2.1% and $p_{81\text{-}160}$=9.5%. Beyond this point, the qualitative (Figs. 13+14) and quantitative (Figs. 12(c_1)-(c_2)) behavior of the trivial and non-trivial 1 paths is quite similar. Indeed, in both cases there is a gradual growth of the preponderance of the shear and transverse extension modes (linear and quadratic) and, in opposite sense a (strong) mode **1** and a (slight) distortional mode contribution reduction – the contribution from the local modes is modest along the whole path and remains more or less constant.

[11] Although no branch switching techniques are implemented in ABAQUS, it was possible to determine the bifurcated solution by varying the maximum arc-length. However, such procedure did not work in all the remaining cases presented in this paper.

(vi) The $w(x)$ configuration along the trivial path exhibits a "perfect" single (distortional) half-wave (akin to the initial geometrical imperfection shape) up to the bifurcation point vicinity (see Figs. 13(a)+(e) for $P/P_{cr}<0.849^{\downarrow}$ and Fig. 16(a_1)). However, progressing further along the equilibrium path $w(x)$ gradually changes from the "perfect" single half-wave to a shape with three "local buckles" in the column central region, like the columns analyzed in sub-section 3.1.1, but unlike in the columns with a "pure" distortional post-buckling behavior (Martins *et al*. 2018a) – in the latter only one "local buckle" appears in the column central region – note, however, that the L/b ratio is also visibly higher (11.8 vs. 8.1). This pattern is particularly visible in the modal displacement profiles $w_6(x)$ (Figs. 13(a) and 14(a)), $w_{5+7-11}(x)$ (Figs. 13(b) and 14(b)), $w_{81-120}(x)$ (Figs. 13(d) and 14(d)) and also $w(x)$ (Figs. 13(e) and 14(e)), as well as in the deformed configurations displayed in Figs. 16(a_2)-(b_3) – this behavioral feature does not stem from L-D interaction. Indeed, the sole difference between the trivial and non-trivial 1 solutions is due to distinct contributions of the local deformations (compare Figs. 13(c) and 14(c)). In the vicinity of the bifurcation point, $w_{12-41}(x)$ exhibits 13 unequal half-waves, instead of 12 half-waves (akin to the critical local buckling mode – Fig. 2(a_3)), because the odd half-wave number favors the interaction with the single distortional half-wave. However, beyond this point, the local deformations become more pronounced at x/L=0.50 in the non-trivial 1 path, while in the trivial path they concentrate in the vicinity of that location. The dominance of the distortional deformations precludes the development of local deformations even when the (distortional) initial imperfection amplitude is very small (*e.g.*, in the $D^1_{0.01mm}$ or $D^2_{0.01mm}$ columns –

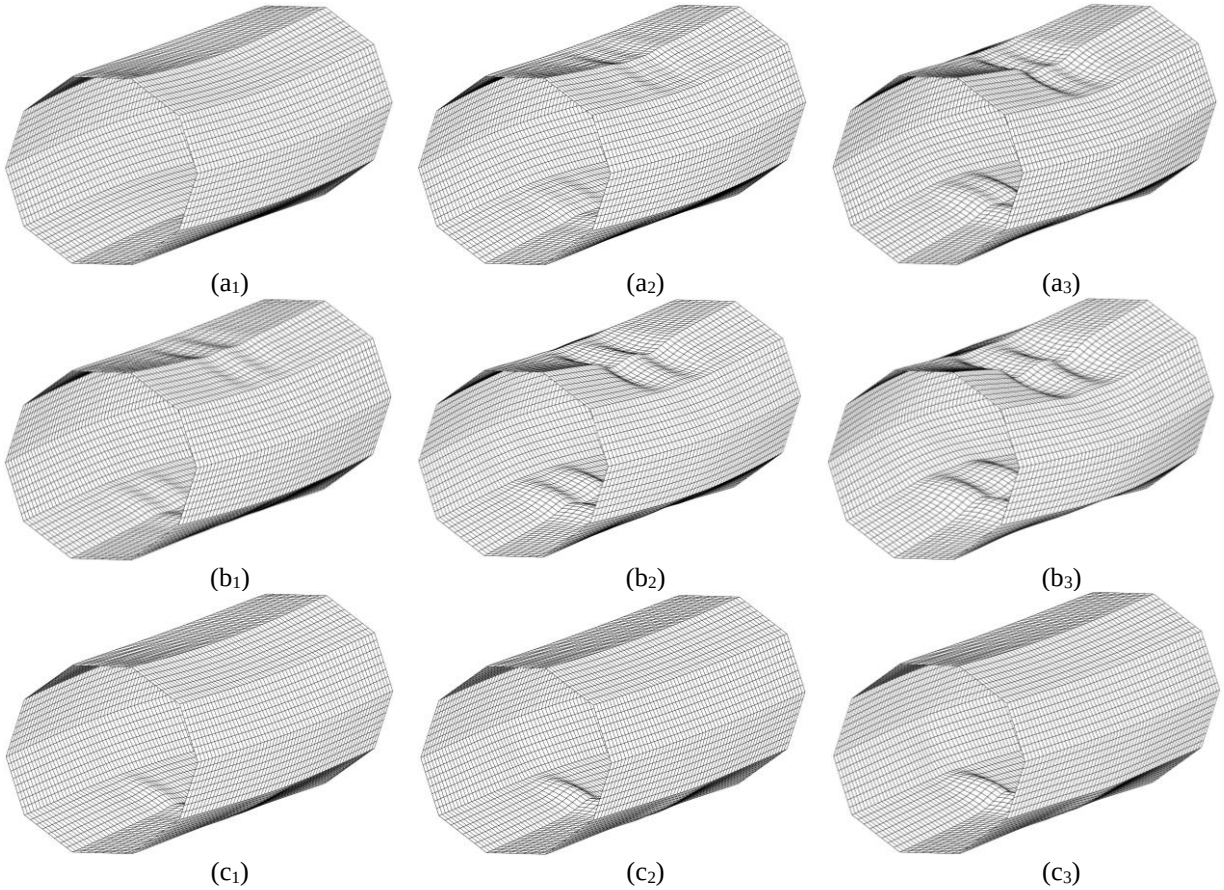

Figure 16: $P_{crD}/P_{crL}\cong 1.0+D^1_{0.5mm}$ column deformed configurations at post-buckling stages defined by P/P_{cr} equal to (a_1) $0.849^{\downarrow}$ (bifurcation point), (a_2) $0.741^{\downarrow}$ and (a_3) $0.512^{\downarrow}$ (trivial path), (b_1) $0.734^{\downarrow}$, (b_2) $0.495^{\downarrow}$ and (b_3) $0.436^{\downarrow}$ (non-trivial 1 path), and (c_1) $0.777^{\downarrow}$, (c_2) $0.549^{\downarrow}$ and (c_3) $0.514^{\downarrow}$ (non-trivial 2 path).

these results are not shown). In summary, the mechanics involved in the behavior of these columns are very similar to those involved in the pure distortional post-buckling behavior (associated with the "trivial" distortional mode), even if the local mode contributions are now slightly more pronounced.

(vii) The mechanics involved in the non-trivial 2 path are completely different from their non-trivial 1 path counterparts, as is clearly illustrated in Figs. 12(c) and 15. The early emergence of flexural deformations (**2**+**3**) shows that a kink develops in the mid-span bottom walls (in this case) along the equilibrium path. Indeed, the above modal participations grow along the equilibrium path, reaching 8.1% at $(w+w_0)/t$=6.05 (P/P_{cr}=0.514$^{\downarrow}$), while the distortional mode contributions decrease from 67.8% to 59.4%. The shear and transverse extension mode participations also increase along the equilibrium path up, to maxima of 9.0% and 10.4%, respectively. On the other hand, the local mode participation is tiny once again – the peak value is 3.4%, reached at $(w+w_0)/t$=3.44 (P/P_{cr}=0.671$^{\downarrow}$).

(viii) The observation of Fig. 15 shows a strong resemblance between the non-trivial 2 path characteristics and the "non-trivial" solution associated with the pure distortional post-buckling behavior (Martins *et al*. 2018a). The only difference is the kink location, which is strongly dependent on the initial geometrical imperfection "rotation" – however, it differs from the case discussed in sub-section 3.1.1. Since the local modes play a minute role in this case ($P_{crD}/P_{crL}\cong$1.0 and distortional imperfections), the post-buckling behavior of these columns is very similar to that of columns exhibiting a pure distortional buckling. Unlike in the trivial and non-trivial 1 paths, significant distortional deformations, due to other distortional modes (besides modes **5**+**6**), emerge, as shown and quantified in Fig.15(c). Moreover, all modal displacement profiles displayed in Fig. 15 exhibit pronounced deformations at the mid-span region, which is naturally reflected in the three deformed configurations displayed in Fig. 16. Like the trivial and non-trivial 1 solutions, this solution corresponds to a distortional post-buckling behavior (or an L-D interactive one with a tiny presence of local deformations), but involving the "non-trivial" distortional mode.

3.1.3 Combined local and distortional initial geometrical imperfections

This sub-section briefly presents and discusses the GNIA results concerning the "trivial" equilibrium path $P_{crD}/P_{crL}\cong$1.0 column containing an initial geometrical imperfection obtained by combining the critical (i) local mode (Fig. 2(a_3)), with an amplitude of 0.5mm, and (ii) the distortional mode 1 (Fig. 2(a_1)), with the lowest amplitude considered in this work (0.01mm) (see the bottom of Fig. 17(a)) – this column is termed $P_{crD}/P_{crL}\cong$1.0+$L_{0.5mm}$+$D^1_{0.01mm}$. The layout of results presented is again similar to that adopted in the previous sub-sections. Fig. 17(a) shows the post-buckling equilibrium path P/P_{cr} vs. $(w+w_0)/t$, where w is now the flexural displacement of the bottom-right wall (see Fig. 17(a)), while Fig. 17(b) depicts the corresponding modal participation diagram, plotted as function of the above displacement. Figs. 18(a)-(c) provide the evolution of the $P_{crD}/P_{crL}\cong$1.0+$L_{0.5mm}$+$D^1_{0.01mm}$ column most relevant modal contributions, namely from (i) the flexural modes ($w_{2+3}(x)$), (ii) the distortional modes ($w_{5-11}(x)$) and (iii) all modes ($w(x)\equiv w_{1-160}(x)$). In addition, three relevant 3D deformed configurations are displayed in Figs. 19(a)-(c), corresponding to the equilibrium states "A", "B" and "C" indicated on the equilibrium path of Fig. 17(a). The observation of these results prompts the following remarks:

(i) The observation of the results presented in Figs. 17-19 shows that this "trivial" post-buckling behavior is completely distinct of that obtained for the P_{crD}/P_{crL}=1.0+$L_{0.5mm}$ column (discussed in Section 3.1.1). Indeed, pronounced distortional deformations emerge after the limit point (see Figs. 17(a) and 18(b)), exhibiting a single half-wave up to the bifurcation point vicinity. Beyond this point, a "kink" begins to develop near the mid-span region (specifically, at $x/L\cong$5/12, *i.e.*, the cross-section location where the bottom-right wall exhibits "outward" local curvatures – similar to those exhibited by the distortional deformations) – at this stage the contributions from the flexural (Fig. 18(a)) and

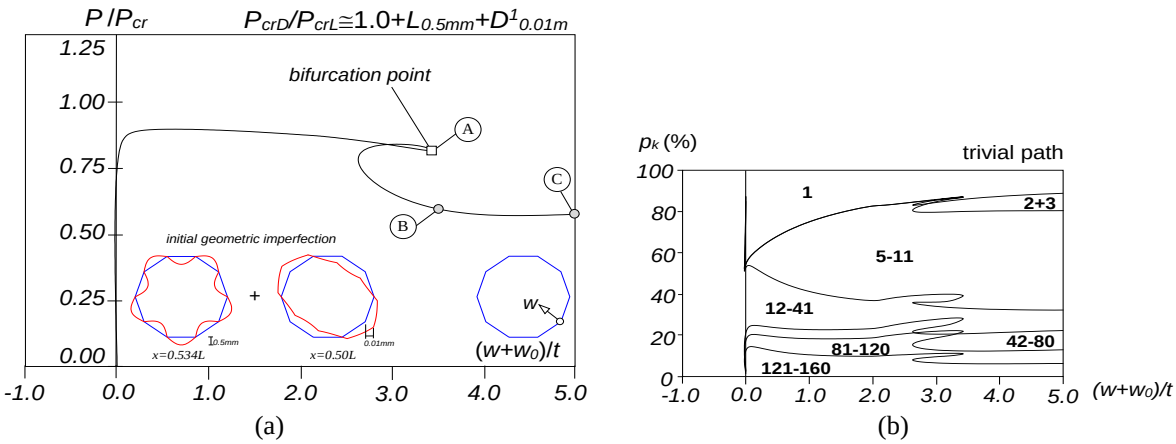

Figure 17: $P_{crD}/P_{crL}\cong 1.0+L_{0.5mm}+D^{1}_{0.01mm}$ column (a) post-buckling equilibrium path P/P_{cr} vs. $(w+w_0)/t$ and associated (b) modal participation diagram.

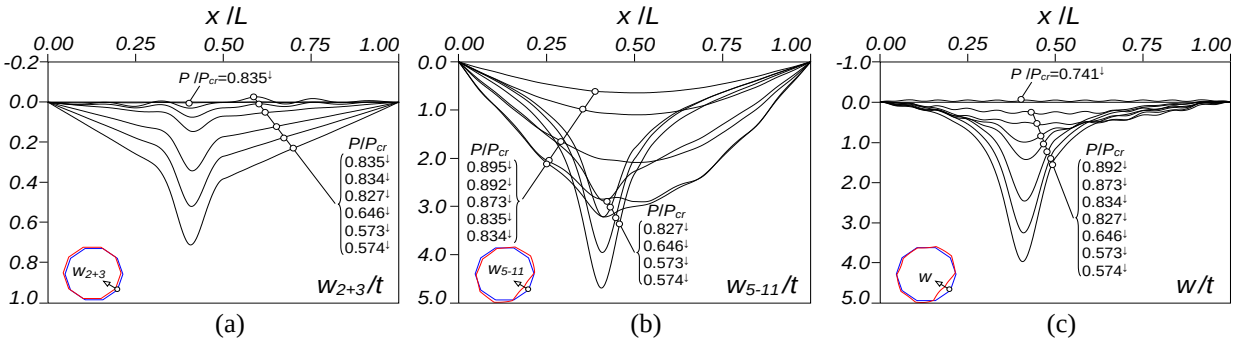

Figure 18: $P_{crD}/P_{crL}\cong 1.0+L_{0.5mm}+D^{1}_{0.01mm}$ column displacement profiles (a) $w_{2+3}(x)$, (b) $w_{5-11}(x)$, (c) $w_{1-160}(x)\equiv w(x)$ – trivial path.

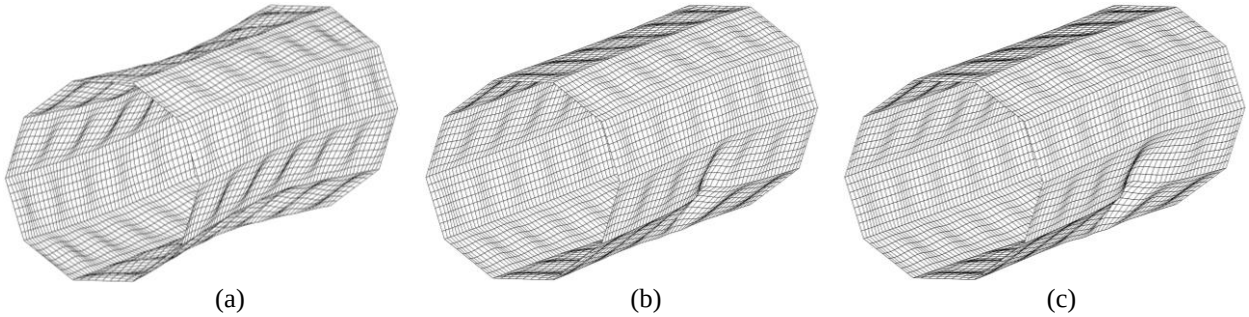

Figure 19: $P_{crD}/P_{crL}\cong 1.0+L_{0.5mm}+D^{1}_{0.01mm}$ column deformed configurations at the post-buckling stages defined by P/P_{cr} equal to (a) $0.814^{\downarrow}$, (b) $0.591^{\downarrow}$, and (c) $0.523^{\downarrow}$.

distortional modes (Fig. 18(b)) are clearly visible. Naturally, this "kink" becomes more pronounced along the equilibrium path – see the deformed configurations in Figs. 19(a)-(c). In other words, this column undergoes L-D interaction involving the "non-trivial" distortional mode (discussed earlier).

(ii) The inclusion of a small initial geometrical imperfection distortional component "breaks" the singular post-buckling behavior exhibited by the $P_{crD}/P_{crL}=1.0+L$ column trivial solution and "restores" the expected L-D interaction behavior. Thus, it may be argued that the surprising "trivial" equilibrium path of the $P_{crD}/P_{crL}=1.0+L$ columns (no L-D interaction), discussed in Sub-section 3.1.1, is very unlikely (or even impossible) to occur in columns containing realistic initial imperfections, which invariably combine local and distortional deformations.

3.2 Secondary distortional-bifurcation L-D interaction

This sub-section addresses the n=10 RCPS P_{crD}/P_{crL}=2.5 column (see Table 1). Although there is a substantial difference between the two competing buckling loads (P_{crL} and P_{crD}), it is well known that the local post-buckling behavior is generally characterized by a high post-critical strength (also in RCPS columns), which means that L-D interaction is bound to occur at advanced loading stages (how advanced naturally depends on the distortional-to-local critical buckling load ratio value). Once more, the presentation of the results is similar to that adopted in sub-section 3.1, making it possible to abbreviate the descriptions. Recalling that only critical-mode (local) initial geometrical imperfections are dealt with (see Section 2), Fig. 20(a) displays column equilibrium paths P/P_{crL} vs. $|(w+w_0)|/t$ up to P/P_{crL}=1.80, where w is the in-plane transverse displacement at the mid-span bottom wall mid-point, caused by the applied load P (w_0 is the corresponding initial value, equal to 0.5, 0.2, 0.1 or 0.01mm). Moreover, Fig. 20(b) shows three equilibrium paths P/P_{crL} vs. $(w+w_0)/t$ (one "trivial" and two "non-trivial") concerning the column with 0.2mm imperfection amplitude (P_{crD}/P_{crL}=2.5+$L_{0.2mm}$), while Figs. 21(a)-(c) display the corresponding modal participation diagrams as a function of P/P_{crL} (Fig. 21(a)) or $(w+w_0)/t$ (Figs. 21(b)+(c)). Figs. 22(a)-(c), provide the evolution, as loading progresses, of the P_{crD}/P_{crL}=2.5+$L_{0.2mm}$ column modal contributions to the displacement $w(x)$ associated with the "trivial" equilibrium path shown in Fig. 20(b), namely the contributions from (i) the local modes ($w_{12\text{-}41}(x)$), (ii) the linear transverse extension modes ($w_{81\text{-}120}(x)$), and (iii) all modes ($w_{1\text{-}160}(x)\equiv w(x)$). Similarly, Figs. 23(a)-(h) and 24(a)-(h) show the same type of results regarding the "non-trivial 1" and "non-trivial 2" equilibrium paths, respectively. In particular, they depict the $w(x)$ modal contributions from (i) the major-axis flexural mode **2** ($w_2(x)$) (Fig. 23(a)) or major and minor-axis flexural modes **2+3** ($w_{2+3}(x)$) (Fig. 24(a)), (ii) the (dominant) distortional mode **5** ($w_5(x)$), (iii) the (less relevant) distortional modes **6-11** ($w_{6\text{-}11}(x)$), (iv) the local modes **12-41** ($w_{12\text{-}41}(x)$), (v) the linear transverse extension modes **81-120** ($w_{81\text{-}120}(x)$) and (vi) all modes ($w_{1\text{-}160}(x)\equiv w(x)$), where w is the mid-bottom wall (Fig. 23) or mid-bottom right wall (Fig. 24) cross-section in-plane transverse displacement. Lastly, Figs. 25(a_1)-(c_3) show three selected deformed configurations per P_{crD}/P_{crL}=2.5+$L_{0.2mm}$ column equilibrium path, as indicated in Fig. 20(b) – states "A", "B" and "C". The observation of all these GBT post-buckling results leads to the following remarks:

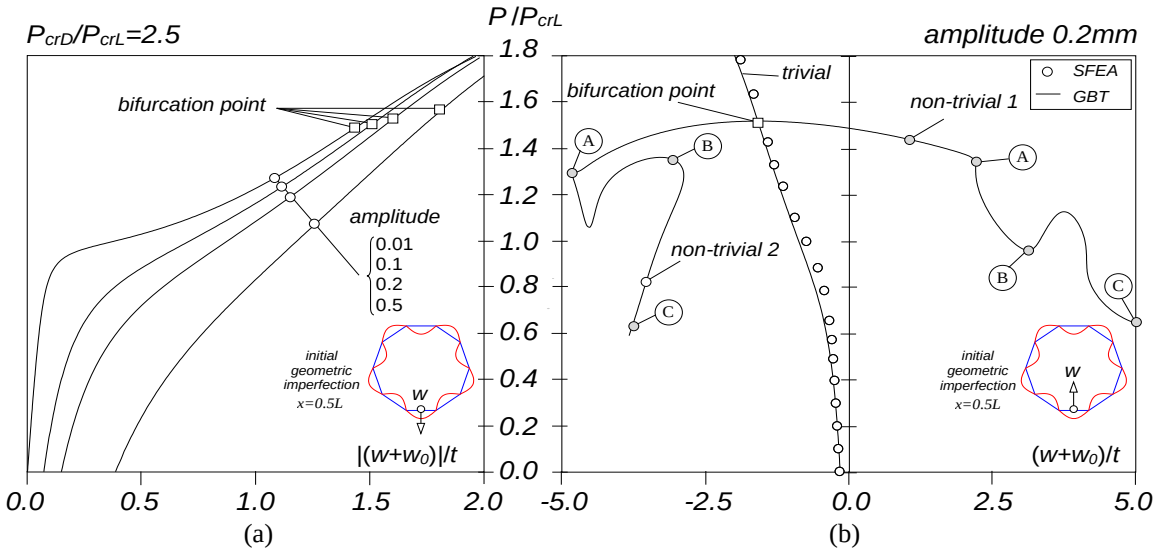

Figure 20: P_{crD}/P_{crL}=2.5 column post-buckling equilibrium paths associated with local initial geometrical imperfections and (a) several amplitudes (0.5, 0.2, 0.1, 0.01mm – trivial solutions) and (b) 0.2mm amplitude (trivial and non-trivial solutions).

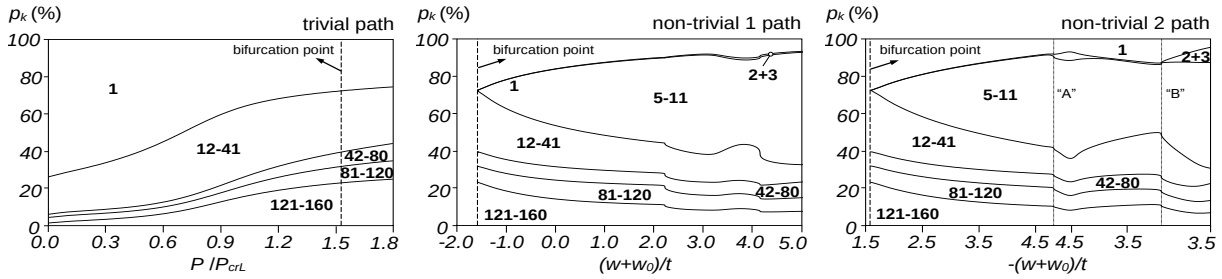

Figure 21: P_{crD}/P_{crL}=2.5+$L_{0.2mm}$ column modal participation diagrams: (a) trivial (b) non-trivial 1 and (c) non-trivial 2 paths.

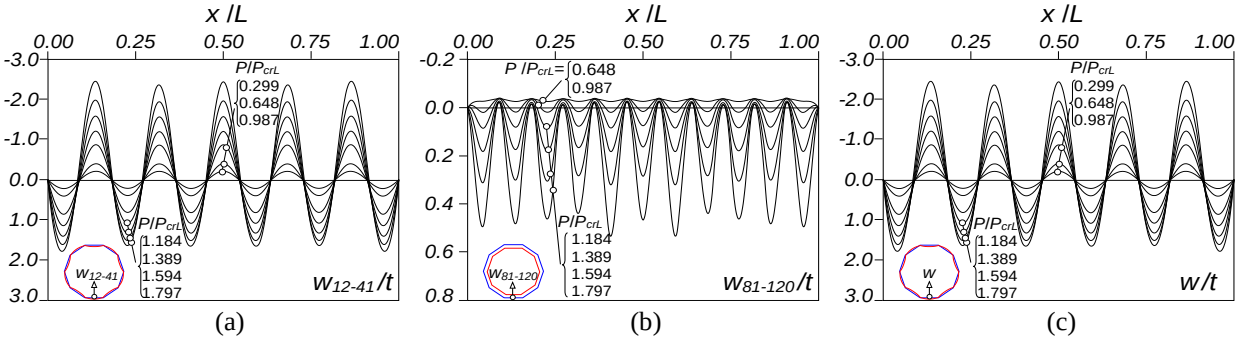

Figure 22: P_{crD}/P_{crL}=2.5+$L_{0.2mm}$ column displacement profiles (a) $w_{12\text{-}41}(x)$, (b) $w_{81\text{-}120}(x)$ and (c) $w_{1\text{-}160}(x)\equiv w(x)$ – trivial path.

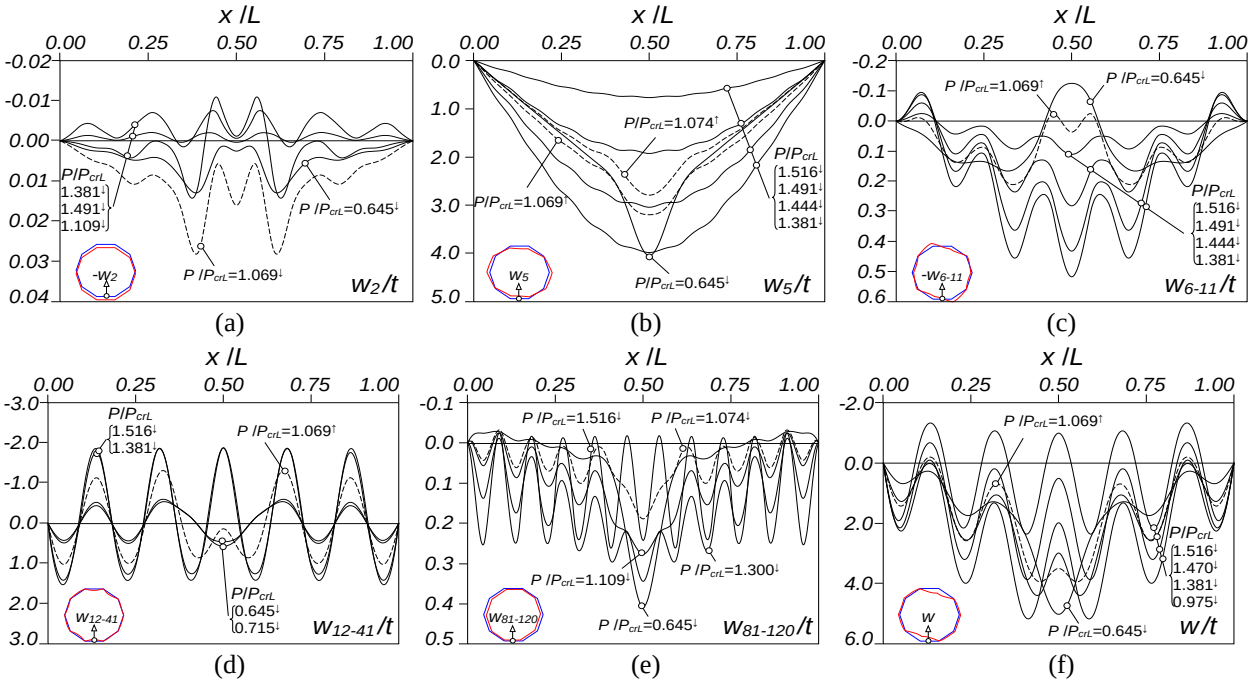

Figure 23: P_{crD}/P_{crL}=2.5+$L_{0.2mm}$ column displacement profiles (a) $w_2(x)$, (b) $w_5(x)$, (c) $w_{6\text{-}11}(x)$, (d) $w_{12\text{-}41}(x)$, (e) $w_{81\text{-}120}(x)$, and (f) $w_{1\text{-}160}(x)\equiv w(x)$ – non-trivial 1 path.

(i) First of all, there is a strong resemblance between the results presented in this sub-section and those discussed in Section 3.1.1 concerning the P_{crD}/P_{crL}=1.0+L columns. Indeed, when local critical-mode initial imperfections are considered (recall also Section 3.1.3), the corresponding equilibrium paths always exhibit high post-critical strength and involve no L-D interaction. The joint observation of the

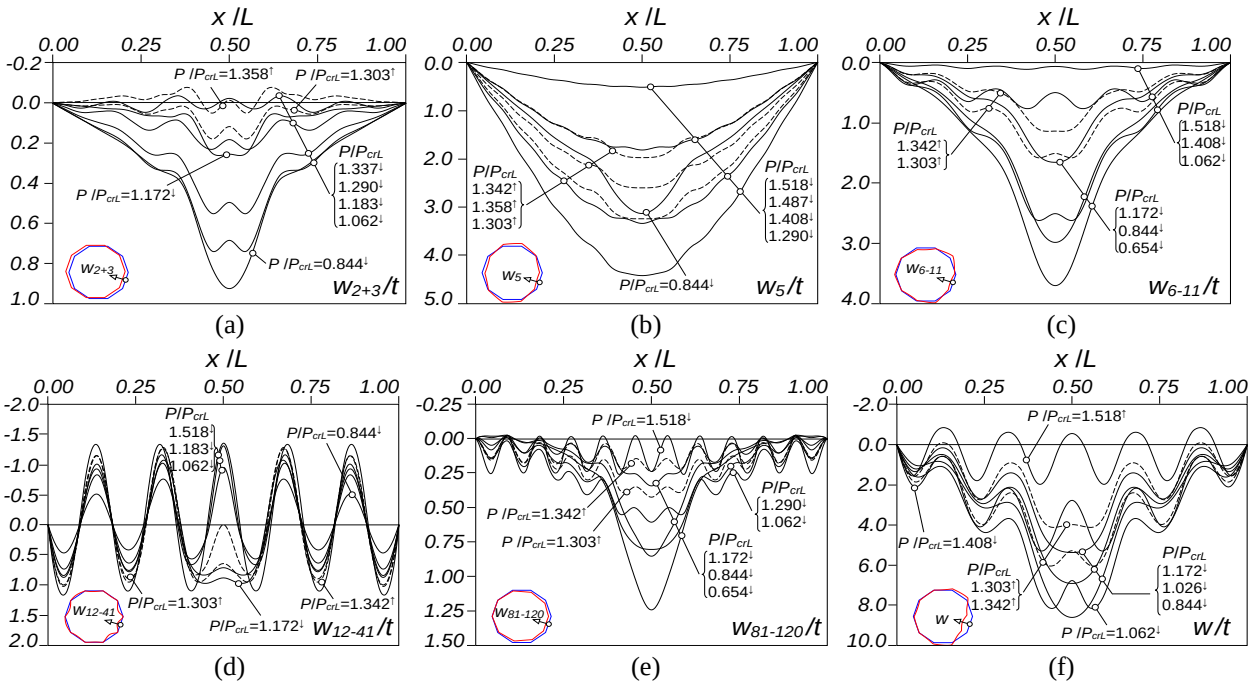

Figure 24: P_{crD}/P_{crL}=2.5+$L_{0.2mm}$ column displacement profiles (a) $w_{2+3}(x)$, (b) $w_5(x)$, (c) $w_{6-11}(x)$, (d) $w_{12-41}(x)$, (e) $w_{81-120}(x)$, and (f) $w_{1-160}(x)\equiv w(x)$ – non-trivial 2 path.

modal participation diagram (Fig. 21(a)), displacement profiles (Figs. 22(a)-(c)) and 3D deformed configurations (Figs. 25(a_1)-(a_3)) evidences the absence of distortional deformations and a similarity with their P_{crD}/P_{crL}=1.0+L column counterpart (Fig. 4(a), Figs. 5(a)-(c), Figs. 8(a_1)-(a_3)), with the n_L nature (even or odd) reflected in the last two figures. The major difference is related to the bifurcation point locations, occurring at advanced post-buckling stages: P/P_{crL}=1.569, 1.529, 1.507, 1.492, respectively for columns with 0.5, 0.2, 0.1 and 0.01mm imperfections – at these bifurcation points, both the GBT and ABAQUS SFEA global stiffness matrices exhibit two negative eigenvalues.

(ii) As expected, distortional deformations emerge in the vicinity of the bifurcation point on the two non-trivial equilibrium paths (see Figs. 21(b)+(c)), mostly due the mode **5** contribution (see Figs. 23(a) and 24(a)) and rapidly become the major source of deformation (see Figs. 21(b)+(c) at the advanced loading stages). However, unlike in the P_{crD}/P_{crL}=1.0+L column, the dominant distortional mode contribution does not exhibit a "perfect" single half-wave (akin to the critical distortional buckling mode), but rather a tiny wavy pattern, up to the equilibrium state "A" (see Fig. 20(b)), most likely due to predominant local deformations taking place in the column near in the bifurcation point – this behavioral feature (deformed configuration switch) occurs despite the substantial difference between P_{crD} and P_{crL}. Since all the results presented in this document are elastic, there is always room for the development of L-D interaction. However, in elastic-plastic columns, the occurrence of this coupling phenomenon is strongly dependent on the yield stress value, *i.e.*, the post-buckling behavior may be either (ii$_1$) "purely" local (no interaction), if the squash load (P_y) falls below the critical bifurcation load or (ii$_2$) affected by L-D interaction, if P_y exceeds that value – in the latter case, a drastic strength erosion may occur and lead to unacceptably low reliability levels (unsafe designs).

(iii) Fig. 20(b) shows another significant difference between the two non-trivial equilibrium paths of the $P_{crD}/P_{crL}\cong$1.0+$L_{0.2mm}$ and 2.5+$L_{0.2mm}$ columns, concerning the most advanced post-buckling stages (*i.e.*, beyond the equilibrium stares "A" – valid for all P_{crD}/P_{crL}=2.5+L columns): a strength increase is observed along these paths, which is related to a localized phenomenon near mid-span.

In the non-trivial 1 path it can be observed that this phenomenon stems from the combined effect of (iii_1) the shape change occurring in $w_{12\text{-}41}(x)$ (Fig. 23(d)) and (iii_2) an amplitude decrease of the distortional deformations (Fig. 23(b)) – a similar type of behavior occurs in the non-trivial 2 path. The column begins by exhibiting eleven (local) half-waves (recall Fig. 2(b)), but as the loading progresses the three central local half-waves (one with "inward" curvature and the two adjacent ones with "outward" curvature) merge quite rapidly into a single "inward" central half-wave (akin to the dominant $w_5(x)$ contribution) – once again, the dominant role played by the distortional deformations in the L-D coupling phenomenon is very clear. Note that this "abrupt" deformed configuration switch does not occur in the P_{crD}/P_{crL}=1.0+L columns, since there is not enough "room" for the development of local deformations as pronounced as those taking place in the P_{crD}/P_{crL}=2.5+L columns (the bifurcation load level twice as large in the latter case). After this localized phenomenon has occurred, $w_{12\text{-}41}(x)$ retains more or less it shape up to equilibrium state "C" – only a slight amplitude decrease is observed (clearly visible in Figs. 21(b)+(c)).

(iv) As discussed in Section 3.1.1, different L-D interactions take place in the two non-trivial equilibrium paths: with the "trivial" distortional mode in the non-trivial 1 path (see Fig. 25(b_3)) and with the "non-trivial" distortional mode in the non-trivial 2 path. In the latter case, only one "kink" develops

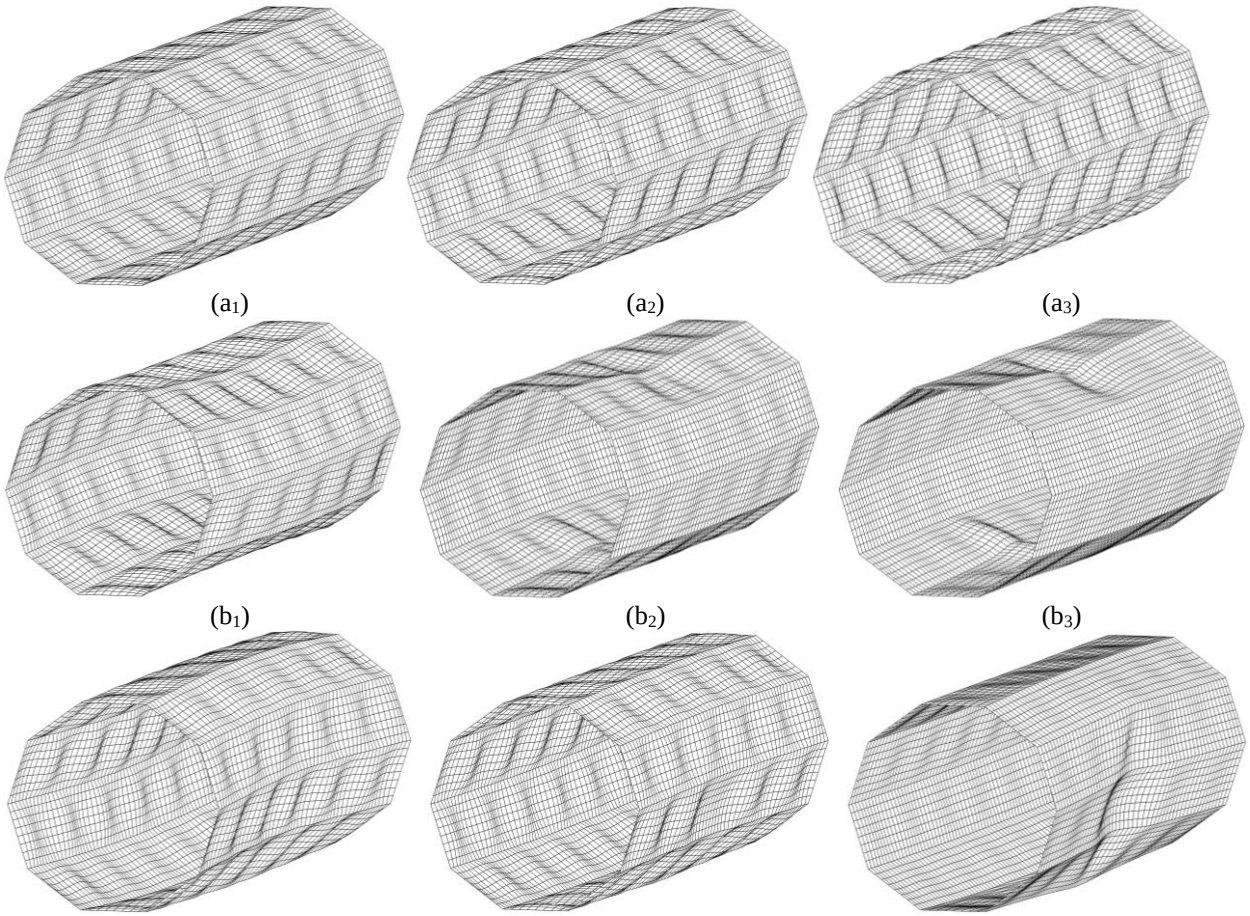

Figure 25: P_{crD}/P_{crL}=2.5+$L_{0.2mm}$ column deformed configurations at equilibrium states defined by P/P_{crL} equal to (a_1) 1.263, (a_2) 1.507 (bifurcation point) and (a_3) 1.813 (trivial path), (b_1) $1.344^{\downarrow}$, (b_2) $0.968^{\downarrow}$ and (b_3) $0.645^{\downarrow}$ (non-trivial 1 path), and (c_1) $1.290^{\downarrow}$, (c_2) $1.342^{\downarrow}$ and (c_3) $0.654^{\downarrow}$ (non-trivial 2 path).

at the mid-span region (see Figs. 24 and 25(c_3)) – recall that two "kinks" occur in the P_{crD}/P_{crL}=1.0+L column. The difference stems exclusively from the n_L number (odd or even) of the column analyzed.

(v) Finally, one last word about the determination of the "border" beyond which L-D interaction ceases to be relevant, for columns with P_{crD}/P_{crL}>1.0 – knowing this "border" is essential to establish accurate and reliable procedures to estimate the failure loads of RCPS columns. Its determination is straightforward: it suffices to perform eigenvalue analyses of the stiffness matrices of columns with distinct (increasing) P_{crD}/P_{crL} ratios, starting at P_{crD}/P_{crL}=2.5 – recall that it was just discussed that this coupling phenomenon may still occur for columns with this ratio value. The minimum P_{crD}/P_{crL} value (higher than 2.5) for which all eigenvalues are positive provides the sought "border": L-D interaction no longer occurs beyond that value (the column post-buckling behavior is purely local).

4. Conclusion

A numerical investigation concerning the elastic geometrically non-linear behavior of simply supported thin-walled regular polygonal tubular columns experiencing local-distortional interaction was reported in this paper. The results presented were obtained by means of Generalized Beam Theory post-buckling analyses, validated whenever possible by ABAQUS shell finite element analyses, and consisted of equilibrium paths, modal participation diagrams, relevant modal displacement profiles, and 2D/3D deformed configurations. After a brief buckling (linear stability) behavior characterization of the selected columns, an in-depth investigation on the mechanics of RCPS columns affected by local-distortional interaction was conducted, with particular attention devoted to characterizing the "true L-D interaction" ($P_{crD}/P_{crL}\cong$1.0) and the "secondary distortional bifurcation L-D interaction" (P_{crD}/P_{crL}>>1.0). Moreover, the effect of different critical-mode initial geometrical imperfections and amplitudes was also examined. Among the various conclusions drawn from this investigation, the following deserve to be highlighted:

(i) The post-buckling behavior of all the RCPS columns analyzed exhibited, in relatively moderate post-buckling stages, loss of uniqueness of the solution, regardless of the P_{crD}/P_{crL} ratio and initial geometrical imperfection shape and/or amplitude. This fact implies that the analysis and design procedures required to capture the above behavior are more complex than those employed to handle common cold-formed steel members (*e.g.*, lipped channel columns) undergoing this same coupling phenomenon.

(ii) The post-buckling behavior of columns with local critical-mode initial geometrical imperfections always exhibited a single solution (trivial/fundamental), characterized by a high post-critical strength (similar to that exhibited by the local post-buckling behavior), regardless of the P_{crD}/P_{crL} ratio value ($\cong$1.0 and 2.5 were the values considered in this study). The analysis of the relevant displacement profiles, expressed in modal form, did not reveal any trace of distortional deformations, which means that no local-distortional interaction takes place. This behavioral feature is rather unique and, to the authors' best knowledge, has never been reported before, even for columns with other cross-sections – see, for instance, the state-of-the art reported by Camotim *et al.* (2018). However, by employing branch switching techniques it was possible to unveil non-trivial solutions associated with the above coupling phenomenon, *i.e.*, distortional deformations gradually emerge and grow along the equilibrium path, until they become the column major source of deformation (see item (v) below). Moreover, it was also shown that, for the $P_{crD}/P_{crL}\cong$1.0 column, the inclusion of a very small distortional (critical-mode) initial geometrical imperfection "breaks" the above singular post-buckling behavior and "restores" the expected occurrence of local-distortional interaction.

(iii) It was shown that, regardless of the P_{crD}/P_{crL} value and initial geometrical imperfection shape and amplitude, there are two variants of local-distortional interaction differing in the distortional post-

buckling nature, *i.e.*, involving either "trivial" (increasing cross-section "ovalization") or "non-trivial" (formation of a localized "kink") distortional deformations. However, both interaction types are strongly influenced by the (iii_1) (distortional) initial geometrical imperfection "rotation", (iii_2) local critical half-wave number (odd or even, leading to longitudinally symmetric or asymmetric deformation patterns, respectively) and (iii_3) local imperfection amplitude. Moreover, depending on the local critical-half-wave number and amplitude, one or two "kinks" may develop (not necessarily at the mid-span regions – note that only columns with a single distortional half-wave (n_D=1) buckling mode were analyzed in this study).

(iv) The true local-distortional interactive and pure distortional post-buckling behaviors are mechanically quite similar, in the sense that both are associated with slightly unstable symmetric bifurcations. This means that the columns exhibiting these two post-buckling behaviors are a little imperfection-sensitive, *i.e.*, an increase in the (distortional) initial imperfection amplitude entails moderate elastic failure load erosion and also a slightly higher applied load level associated with the bifurcation point.

(v) Regardless of the critical distortional-to-local buckling ratio and initial geometrical imperfection shape, the mechanics underlying L-D interaction are governed by the distortional deformations, whose influence clearly outweighs that of all other deformation patterns – the local deformations always play a minor/secondary role. This behavioral feature is more pronounced in the columns with $P_{crD}/P_{crL}>>1.0$ (local buckling precedes distortional buckling by a large amount). This fact explains the closeness between the responses of (v_1) columns exhibiting a pure distortional post-buckling behavior and (v_2) columns with $P_{crD}/P_{crL}\cong 1.0$ that contain distortional initial imperfections. It is worth noting that similar conclusions were reached in the context of columns with (open) lipped cross-sections experiencing this same coupling phenomenon.

Acknowledgments

The financial support of the European Commission, through the Research Fund for Coal and Steel project RFCS-2015-709892, "Overall-Slenderness Based Direct Design for Strength and Stability of Innovative Hollow Sections" (HOLLOSSTAB), is gratefully acknowledged.

References

Bebiano R., Camotim D., Gonçalves R. (2018). GBTUL 2.0 – A second-generation code for the GBT-based buckling and vibration of thin-walled members. *Thin-Walled Structures*, **124**(March), 235-257.

Bebiano R., Gonçalves R., Camotim D. (2015). A cross-section analysis procedure to rationalize and automate the performance of GBT-based structural analysis. *Thin-Walled Structures*, **92**(July), 29-47.

Borst R., Crisfield M.A., Remmers J.J.C., Verhoosel C.V. (2012). *Non-linear Finite Element Analysis of Solids and Structures* (2nd edition), John Wiley & Sons Ltd (Chichester).

Camotim D., Basaglia C., Bebiano R., Gonçalves R., Silvestre N. (2010a). Latest developments in the GBT analysis of thin-walled steel structures, *Proceedings of International Colloquium on Stability and Ductility of Steel Structures* (SDSS'Rio 2010 – Rio de Janeiro, 8-10/9), E. Batista, P. Vellasco, L. Lima (eds.), 33-58 (Vol. 1).

Camotim D., Basaglia C., Silva N.F., Silvestre N. (2010b). Numerical analysis of thin-walled structures using Generalised Beam Theory (GBT): recent and future developments, *Computational Technology Reviews*, vol. 1, B. Topping *et al.* (ed.), Saxe-Coburg (Stirlingshire), 315-354.

Camotim D., Dinis P.B., Martins A.D., Young B. (2018). Review: Interactive behaviour, failure and DSM design of cold-formed steel members prone to distortional buckling, *Thin-Walled Structures*, **128**(July), 12-42.

Gonçalves R., Ritto-Corrêa M., Camotim D. (2010). A new approach to the calculation of cross-section deformation modes in the framework of Generalized Beam Theory, *Computational Mechanics*, **46**(5), 759-781.

Gonçalves R., Camotim D. (2012). Geometrically non-linear Generalised Beam Theory for elastoplastic thin-walled metal members, *Thin-Walled Structures*, **51**(February), 121-129.

Gonçalves R., Camotim D. (2013a). On the behaviour of thin-walled steel regular polygonal tubular members, *Thin-Walled Structures*, **62**(January), 191-205, 2013.

Gonçalves R., Camotim D. (2013b). Elastic buckling of uniformly compressed thin-walled regular polygonal members, *Thin-Walled Structures*, **71**(October), 35-45.

Gonçalves R., Camotim D. (2013c). Buckling behaviour of thin-walled regular polygonal tubes subjected to bending or torsion, *Thin-Walled Structures*, **73**(December), 185-197.

Gonçalves R., Camotim D. (2014). The vibration behaviour of thin-walled regular polygonal tubes. *Thin-Walled Structures*, **84**(November), 177-188.

Gonçalves R., Camotim D. (2016). On the first-order and buckling behaviour of thin-walled regular polygonal tubes, *Steel Construction – Design and Research*, **9**(4), 279-290.

Gonçalves R., Bebiano R., Camotim D. (2014). On the shear deformation modes in the framework of generalized beam theory, *Thin-Walled Structures*, **84**(November), 325-334.

Martins A.D., Dinis P.B., Camotim D., Providência P. (2015). On the relevance of local-distortional interaction effects in the behaviour and design of cold-formed steel columns, *Computers & Structures*, **160**(November), 57-89.

Martins A.D., Gonçalves R., Camotim D. (2018a). On the local and distortional post-buckling behaviour of thin-walled regular polygonal tubular columns, *submitted for publication*.

Martins A.D., Camotim D., Gonçalves R., Dinis P.B. (2018b). On the mechanics of local-distortional interaction in thin-walled lipped channel columns, *Thin-Walled Structures*, **125**(April), 187-202.

Martins A.D., Camotim D., Gonçalves R., Dinis P.B. (2018c). On the mechanics of local-distortional interaction in thin-walled lipped channel beams", *Thin-Walled Structures*, **128**(July), 108-125.

Martins A.D., Camotim D., Gonçalves R., Dinis P.B. (2018d). Enhanced geometrically non-linear Generalized Beam Theory (GBT) formulation: derivation, numerical Implementation and illustration, *Journal of Engineering Mechanics* (ASCE), **144**(6), paper 04018036 (20 pages).

Schardt R. (1989). *Verallgemeinerte Technische Biegetheorie*, Berlin, Springer-Verlag. (German)

Timoshenko S., Gere J. (1961). *Theory of Elastic Stability*, New York, McGraw-Hill.

Wittrick W., Curzon P. (1968). Local buckling of long polygonal tubes in combined compression and torsion, *International Journal of Mechanical Sciences*, **10**(10), 849-857.